Thermal and structural characterization of Fipronil

by

Dennis Simbarashe Moyo

11327414

Supervisor: Prof. Walter Wilhelm Focke

Co-supervisors: Prof. Elizabet Margaretha van der Merwe

& Prof. Melanie Rademeyer

Submitted in fulfilment of the requirements for the degree

Philosophiae Doctor (PhD in Chemistry)

in the Faculty of Natural and Agricultural Science

Department of Chemistry

University of Pretoria

June 2023

Declaration of Originality

I, **Dennis Simbarashe Moyo**, declare that the thesis, which I hereby submit for the degree of **Doctor of Philosophy** at the University of Pretoria, is my own work and has not previously been submitted by me for a degree at this or any other tertiary institution.

1. I understand what plagiarism is and am aware of the University's policy in this regard.
2. I declare that this thesis (e.g. essay, report, assignment, dissertation, thesis, etc.) is my own original work. Where other people's work has been used (either from a printed source, internet or any other source), this has been properly acknowledged and referenced in accordance with departmental requirements.
3. I have not used work previously produced by another student or any other person to hand in as my own.
4. I have not allowed, and will not allow, anyone to copy my work with the intention of passing it off as his or her own work.

Signature: Dennis Moyo.....

Date: 06/02/2024.....

Acknowledgements

I would like to express my deep appreciation to the individuals listed below for their invaluable contributions that have played a crucial role in the successful completion of this project:

Prof. Walter W. Focke (Project Supervisor)

Prof. Liezel M. van der Merwe (Project Supervisor)

Prof. Melanie Rademeyer (Project Supervisor)

Dr Antonio B. Mapossa

Dr Frederick Malan

Dr Maria Atanasova

Furthermore, I extend my heartfelt gratitude to the Institute of Applied Materials (IAM), the University of Pretoria Centre for Sustainable Malaria Control (UPCSMC), and the Department of Higher Education and Training (DHET) for their generous financial support, which has enabled me to pursue my PhD studies.

Lastly, I would like to express my sincerest thanks to my parents, whose unwavering love, encouragement, and support have been instrumental throughout my academic journey. Their belief in me has been a constant source of motivation, and I am truly grateful for their presence in my life.

And finally, I would like to acknowledge my wife, Dr Ruvimbo Chipunza, for her unwavering support and constant encouragement. Her presence by my side has been a source of strength, and I am truly grateful for her unwavering belief in my abilities.

Academic Output

Journal papers

1. Dennis Simbarashe Moyo, Elizabet Margaretha van der Merwe, Melanie Rademeyer, Frederick Pieter Malan, Maria T Atanasova, António Benjamim Mapossa, Walter Wilhelm Focke, 2023. Characterizing the thermal phase behaviour of fipronil polymorphs. *Journal of Thermal Analysis and Calorimetry*, pp 1-17. Available online https://doi.org/10.1007/s10973-023-12198-x.
2. Dennis Simbarashe Moyo, António Benjamim Mapossa, Elizabet M van der Merwe, Melanie Rademeyer, Walter Wilhelm Focke, 2002. TGA investigation of the volatilization of fipronil at elevated temperatures. *Thermochimica Acta*, 718: pp. 179379. Available online https://doi.org/10.1016/j.tca.2022.179379.
3. Mapossa, António B., Jorge López-Beceiro, Ana María Díaz-Díaz, Ramón Artiaga, Dennis S. Moyo, Thabang N. Mphateng, Walter W. Focke, 2021. Properties of Mosquito Repellent-Plasticized Poly (lactic acid) Strands. *Molecules 26*, 19: pp. 5890. Available online https://www.mdpi.com/1420-3049/26/19/5890.
4. António Benjamim Mapossa, Mthoko Mayibongwe Sibanda, Dennis Moyo, Taneshka Kruger, Walter Wilhelm Focke, René Androsch, Regine Boldt & James Wesley-Smith, 2021. Blooming of insecticides from polyethylene mesh and film, *Transactions of the Royal Society of South Africa*, 76:2, pp. 127-136. Available online https://doi.org/10.1080/0035919X.2021.1900950.

5. Mapossa, António B., Dennis Moyo, James Wesley-Smith, Walter W. Focke, and René Androsch, 2020. Blooming of chlorfenapyr from polyethylene films. In AIP Conference Proceedings, vol. 2289, 1: pp. 020036. AIP Publishing LLC. Available online https://aip.scitation.org/doi/pdf/10.1063/5.0028438.

International conference and workshop contributions

1. Dennis S. Moyo, Elizabet M. van der Merwe, Frederick P. Malan, Melanie Rademeyer, Antonio B. Mapossa, Maria Atanasova, Walter W. Focke. Thermal and ctructural characterizaton of fipronil. 3rd Journal of Thermal Analyisis and Calorimetry Conference & 9th V4 (Joint Czech-Hunarian-Polish-Slovakian) Thermoanalytical Conference, 20-23 June 2023. Balatonfured, Hungary. Poster presentation.
2. Dennis S. Moyo, Elizabet M. van der Merwe, Frederick P. Malan, Melanie Rademeyer, Antonio B. Mapossa, Maria Atanasova, Walter W. Focke, 2021. Characterizing the thermal behaviour of fipronil, 17th International Congress on Thermal Analysis and Calorimetry, 29 Aug. – 2 Sept. 2021, on-line conference. Oral presentation.
3. Workshop titled "German-African Cooperation Projects in Infectiology". University of Pretoria, South Africa, Eduardo Mondlane University-Mozambique Martin Luther University Halle-Wittenberg-Germany, and Leibniz Institute of Polymer Research Dresden (IPF)-Germany. March 2020, Pretoria, South Africa.
4. Workshop titled "Applied Polymer Technology in different fields". University of Pretoria, South Africa, and Leibniz Institute of Polymer Research Dresden (IPF)-Germany. February 2019, Pretoria, South Africa.

National conference and workshop contributions

1. Dennis S Moyo, António B Mapossa, Melanie Rademeyer, Liezel van der Merwe, Walter W Focke (2023) Isothermal TGA investigation of the sublimation of fipronil at

polymer processing temperatures, 44th SACI National Convention, 8-13 Jan. 2023, Stellenbosch, South Africa. Oral presentation.

Summary

Fipronil is a widely used insecticide which exerts selective toxicity towards the GABA receptors of insects and has no known pesticide resistance in target insects. This, in turn, has led to the increase in the usage of fipronil as an alternative to commonly used pesticides in residential, industrial, commercial and agricultural settings.

In this study, fipronil was considered for use as the chemical active in a controlled-release polymer system applied as alternative to indoor residual spraying in the fight against malaria. However, before incorporating the insecticide in a polymer, the vaporization and polymorphic behaviour of fipronil had to be studied. This information is important in providing guidance for the implementation of suitable safety measures during polymer processing to prevent exposure or contact to substances which could potentially harm one's health. On the other hand, polymorphism affects various physicochemical properties like the melting point, solubility, stability and manufacturability of a compound, which are extremely important for quality control and assurance.

Differential scanning calorimetry (DSC), thermogravimetric analysis (TGA), powder X-ray diffraction (PXRD) and single crystal X-ray diffraction (SCXRD) were used to study the vaporisation and polymorphic behaviour of fipronil. Sublimation and evaporation rates were determined using isothermal TGA. From these results, vapour pressures were deduced on the assumption that the fumes behaved like ideal gases and that mass loss was controlled by diffusion through the gas present in the partially-filled crucible. For the latter process, the diffusion coefficient was estimated using the Fuller correlation. Results obtained using benzoic acid as the calibration standard suggested that it is possible to estimate vapour pressures to

within 12% with this TGA method. The enthalpies of sublimation and of evaporation were determined as 120 ± 4 and 72 ± 5 kJ mol^{-1}, respectively.

Polymorphic behaviour was studied through a systematic comparison of the thermal and structural properties of different crystal forms, including those obtained in this study and in literature. DSC was particularly useful in differentiating between two different crystal forms found in the as-received neat fipronil. Two polymorphs were successfully separated through sublimation of neat fipronil. A metastable, lower melting polymorph and a thermodynamically stable, higher melting form were obtained in the sublimate and residue, respectively. The lower melting polymorph was found to be unstable at high heating rates, with evidence suggesting a solid-solid phase transition to the stable form at low heating rates.

Solvent recrystallization of neat fipronil in acetonitrile, acetone, ethyl acetate and methanol yielded five different crystal forms of fipronil. TGA curves revealed that all five crystal forms, except for the acetone-derived sample, were solvate pseudo-polymorphs exhibiting solvent loss between 60 and 100 °C. The acetone-derived sample was found to be a hemihydrate exhibiting mass loss at 120 °C. SCXRD studies revealed that three of the five forms had similar structural characteristics, while the other two forms differed notably from each other and the rest of the structures. Despite these differences, all five forms exhibited near-identical intra- and intermolecular hydrogen bond networks.

The sublimation and evaporation enthalpies were successfully determined and the data indicates that fipronil will likely sublime at polymer processing conditions above 150 °C. The study also demonstrated, by DSC analysis, that the lower melting form in the neat, as-received fipronil would be converted to the high melting, thermodynamically stable form at the polymer processing conditions.

Table of Contents

List of Tables

List of Figures

List of Acronyms and Abbreviations

A	cross-sectional surface area of the sample cup
ATR	attenuated total reflection
β	heating rate (°C min^{-1})
CM	crystalline modification
°C	degrees Celsius
°C min^{-1}	degrees Celsius per minute
ρ	density (g cm^{-3})
D_{AB}	diffusion coefficient (m^2 s^{-1})
DDT	dichlorodiphenyltrichloroethane
DSC	Differential scanning calorimetry
DTG	Derivative thermogravimetry
FTIR	Fourier transform infrared spectroscopy
G	Gibbs free energy
H	enthalpy (J)
HSM	Hot stage microscopy
IRS	Indoor residual spraying
ITN	Insecticide treated net
J g^{-1}	Joules per gram
kJ mol^{-1}	kilojoules per mole
µL	microlitres
mg	milligrams
mL min^{-1}	millilitres per minute
M_i	molar mass of compound I (g mol^{-1})
MW	molecular weight (g mol^{-1})
N_2	nitrogen gas
P	pressure (atm)
P_{AB}	sample vapour pressure at absolute temperature
PXRD	powder X-ray diffraction

R	gas constant (8.3145 J $mol^{-1}K^{-1}$)
S_{AB}	nitrogen permeability of the evaporating substance (Pa m^2 s^{-1})
SCXRD	single crystal X-ray diffraction
T	temperature (°C)
T_b	boiling temperature (°C)
T_m	melting temperature (°C)
T_s	desolvation temperature (°C)
TGA	Thermogravimetric analysis
Vi	diffusion volume of compound i (cm^3 mol^{-1})
WHO	World Health Organization
wt-%	percentage by weight
XRD	X-ray diffraction
z	the depth of the gas-filled part of the sample cup
ΔH_m	melting enthalpy (J g^{-1})
ΔH_c	crystallization enthalpy (J g^{-1})

Chapter 1

Introduction

1.1 Introduction

This chapter provides an overview of the essential aspects to understanding the research project at hand. It begins by providing a detailed background that contextualizes the study and explains its relevance and significance. Next, a problem statement is outlined as well as the broad and specific goals of the research project through the aims and objectives. In addition, the chapter explains the scope and limitations of the study, clarifying the boundaries and extent of the research project. Finally, an overview of the thesis chapters is given.

1.2 Research background and problem statement

Malaria is a mosquito-borne disease caused by a parasite of the genus *Plasmodium*. It is endemic to tropical regions and sub-tropical regions of Africa, Asia, Central and South America. Six species of the malaria parasite infect human beings i.e. *Plasmodium malariae, Plasmodium vivax, Plasmodium falciparum, Plasmodium knowlesi, Plasmodium ovale curtisi* and *Plasmodium ovale wallickeri* (Miller et al., 1994, Milner, 2018). Infection by *P. falciparum* is the deadliest, accounting for the majority of malaria-related mortality and morbidity. Globally, approximately 241 million cases of malaria occurred in 2020 – 95% (228 million) of these cases were in the African region, with an estimated 627 000 malaria-related deaths (World Health Organization, 2021).

Vector control is the implementation of various strategies to reduce the transmission of malaria by mosquitoes, the primary vectors (or carriers) of malaria (Karunamoorthi, 2011). These strategies typically involve reducing the mosquito population in an area and minimizing

human-mosquito contact through the use of insecticides, mosquito nets, and environmental management strategies. Malaria vector control is an essential component of malaria control and elimination programs worldwide (Karunamoorthi, 2011, Gari and Lindtjørn, 2018). It is recognized as the most effective means of controlling malaria transmission. It's primary objectives are to reduce human-vector contact, thereby stopping transmission, and lowering the vector population (Ariey et al., 2019, Najera and Zaim, 2001). A successful approach combines chemical, biological, physical, genetic and environmental management methods (Ariey et al., 2019). Among these approaches, the use of insecticides targeting adult-stage mosquitoes is the primary control tool in the majority of vector control programs worldwide (Raghavendra et al., 2011). Key chemical control interventions applicable for populations at risk of malaria are indoor residual spraying (IRS) and insecticide-treated nets (ITNs) (World Health Organization, 2019).

IRS use has declined since the 1980's due to concerns regarding the safety and environmental hazards of dichlorodiphenyltrichloroethane (DDT) (Najera and Zaim, 2001). Most World Health Organization (WHO) approved alternatives to DDT are highly volatile, resulting in an early loss in residual efficacy. In addition, spraying is often inefficient, primarily due to loss of the active agent by various degradation processes such as volatilization, evaporation, photolytic and hydrolytic degradation. Consequently, repeated application of the insecticide becomes necessary to maintain the desired concentration, which in turn lead to health and environmental problems due to excessive exposure to large amounts of insecticides.

ITN's make use of controlled release systems which present several benefits over indoor residual spraying (IRS). ITNs release insecticides gradually, minimizing people's exposure to insecticides over time. Furthermore, ITNs remain effective for extended periods, even at low doses, which can span up to three years. This prolonged efficacy helps to prevent the

development of insecticide-resistant mosquito populations and mitigates the environmental impact associated with insecticide use (Lengeler et al., 1996, Lengeler et al., 2007).

Researchers have explored the use of wall or ceiling linings composed of biodegradable polymer-based controlled-release systems, similar to those found in ITN's, as alternative vector control methods to indoor residual spraying (Mapossa et al., 2021, Mapossa et al., 2020, Madzorera et al., 2019). In a study by Mapossa et al. (2021), the insecticides alphacypermethrin, chlorfenapyr and fipronil were successfully incorporated into polyethylene mesh and films at concentrations ranging from 0.5% to 2.5% by weight. The release of the insecticides from the films was tracked over time using FTIR-ATR. It was observed that all three insecticides completely bloomed out of the films within less than four days of oven ageing at 40 °C. Additionally, the study revealed that fipronil demonstrated the highest solubility among the three pesticides used in polyethylene. This finding suggests that fipronil has the potential to be used in a tri-layer film, where the insecticide would be contained within the innermost layer, while the outer two layers would function as low permeability membranes, regulating the release rate (Fig. 1.1).

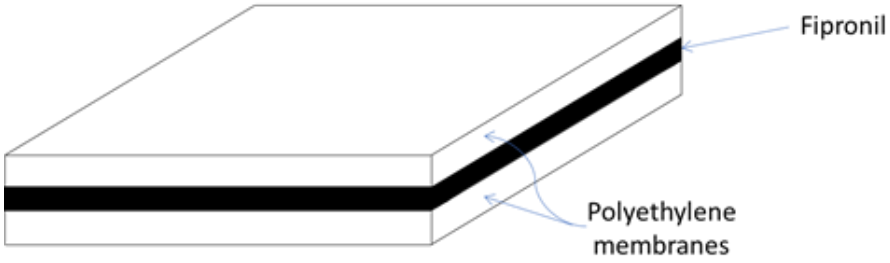

Figure 1.1. Polyethylene tri-layer film with fipronil entrapped in the middle layer.

In order to ensure the safety of the film blowing process, it is essential to examine the thermodynamic characteristics of fipronil at the temperatures used in polymer processing.

During the conversion of the polyethylene, Mapossa et al. (2020) observed formation of fipronil crystals on the die face of the extruder. Fipronil, like other pesticides, poses a significant health risk if it comes into contact with the skin or is inhaled. This constitutes a severe health hazard (Singh et al., 2018, Menon et al., 2002). The risk of exposure becomes even more pronounced when a toxic compound is present in the air during processing. Therefore, a comprehensive understanding of the thermodynamic properties and vaporization process of fipronil is crucial in establishing appropriate safety measures to prevent exposure or contact with the toxic substance during the production of polymer products containing fipronil.

Another noteworthy finding was the significant differences in the FTIR spectra of fipronil after the melt extrusion compared to the spectra of the neat, as-received fipronil. Fipronil is known to exist in several polymorphic/pseudopolymorphic forms; however, there is no consensus on the actual crystal structure of the solvent-free polymorphs. The presence of two melting points in the DSC curve of a purportedly pure polymorph further adds to the complexity of the situation (Saxell et al., 2011, Saxell et al., 2012, Saxell et al., 2013, Zamir, 2013, Saxell et al., 2014, Park et al., 2017, Saxell et al., 2018). Polymorphism, which refers to structural differences within a compound, is a topic of significant interest due to its effects on various properties such as melting and sublimation temperatures, heat capacity, density, solubility, dissolution rates, pharmacological activity, particle size, stability, and manufacturability (Roy et al., 2005, Bhatia et al., 2018).

1.4 Aims and objectives

Given the aforementioned health and safety concerns and the limited understanding of fipronil's polymorphic behaviour in existing literature, the primary aims of this study were to analyse the sublimation and vaporization behaviour of fipronil, and to elucidate its polymorphic behaviour in the temperature range of 150-220°C. The main objectives of this study were as follows:

1. To determine the thermal characteristics of fipronil, specifically its sublimation and evaporation patterns at temperatures encountered during the conversion processes utilized to produce tri-layer films containing fipronil as the contact insecticide.

2. To extract the vapour pressure data and determine the enthalpies of sublimation and vaporization for fipronil from isothermal TGA curves.

3. To isolate and characterise different crystal forms of fipronil through recrystallization from different solvents.

4. To investigate the polymorphic behaviour of fipronil using a systematic comparison of thermochemical and structural properties of various crystal forms of fipronil obtained in this study and reported in the literature.

1.5 Scope and limitations of the study

Direct thermogravimetric measurements were used to ascertain the mass loss per unit time at set isothermal temperatures. The instrumental parameters related to the sublimation rate were determined using benzoic acid, whose vapour pressure is well-known. The temperature-dependent sublimation and vaporization of fipronil were then determined by utilizing the Clausius-Clapeyron vapour pressure equation, assuming ideal gas behaviour, constant enthalpy of phase transition, and negligible molar volume of the condensed state relative to the vapour phase.

In order to understand the polymorphic behaviour of fipronil, a thorough investigation applying several analytical techniques providing complementary insights into the structural properties was applied. The crystal forms analysed in this study were obtained by recrystalizing fipronil from acetone, acetonitrile, ethyl acetate and methanol. Differential Scanning Calorimetry (DSC), Thermogravimetric Analysis (TGA), powder X-ray Diffraction (PXRD) and single Crystal X-ray Diffraction (SCXRD) were used to assess the polymorphic behaviour of fipronil.

This study does not include investigations or discussions regarding the following:

- Optimization of crystallization conditions for obtaining the various crystal forms of fipronil.
- Separation and purification of the mixtures of fipronil crystal forms obtained from recrystallization.
- Concomitant thermophysical transitions, such as pre-melting and onset of thermochemical degradation in the mass loss data.
- Variation of the heating rate used to reach the isothermal temperature during TGA measurements.

1.6 Structure of Thesis

This thesis consists of the following chapters:

Chapter 1 The problem statement and objectives of the investigation are introduced.

Chapter 2 Literature review which provides background information on malaria vector control, fipronil, vapour pressure estimation and polymorphism.

Chapter 3 The experimental procedures, materials and methods are presented.

Chapter 4 A report and discussion of the sublimation characterization and vapour pressure estimation of fipronil using isothermal thermogravimetric analysis.

Chapter 5 A report and discussion of the single crystal X-ray diffraction (SCXRD) characterization of fipronil crystal forms obtained in this study.

Chapter 6 Characterization of the thermal phase behaviour of fipronil using TGA and DSC analysis.

Chapter 7 Conclusions and recommendations for future work based on the findings of this study.

Chapter 2

Literature Review

2.1 Introduction

This chapter provides an in-depth literature review which provides a comprehensive understanding of relevant research topics and theories surrounding them, in order to better inform the subsequent analysis and discussion. It begins with an overview of the history of malaria and the methods used for controlling malaria vectors. In addition, it familiarizes readers with three key areas that are being examined in this study: fipronil, polymorphism, and vapour pressure estimation.

2.2 A brief history of malaria

Malaria has plagued humans throughout historical antiquity, with evidence of its presence dating back almost 5000 years in ancient Chinese medical records. Scriptures containing references to intermittent fevers and splenomegaly, almost certainly indicating malaria, have been quoted in Brahminic (2,800 to 1,900 years ago) and Vedic texts (3,500 to 2,800 years ago) from India (Carter and Mendis, 2002). Egyptian and Sumerian texts from 3,500 to 4,000 years ago made frequent references to deadly epidemic fevers. Alexander the Great is believed to have died from malaria in 323 B.C. en route to India. Malaria also appeared in the writings of the Greeks from around 500 B.C., most notably in works attributed to Hippocrates, who mentioned different forms of malaria, including *febris tertian* (every third day) and *febris quartana* (every fourth day) (Carter and Mendis, 2002, Gaur et al., 2016).

At the advent of the Christian era, malaria was common in southern Europe, around the shores of the Mediterranean, across the Arabian Peninsula, and in China, Korea, Manchuria, Central, South, and Southeast Asia, and Japan. At the end of the 15th century, European traders and

soldiers brought several malaria parasites, within their bodies, to the Caribbean and parts of South and Central America. By 1850 A.D., malaria was widespread in all parts of the subtropical, tropical and temperate regions of North and South America. From the time of Christopher Columbus' expeditions until the mid-19th century, more deaths were recorded due to malaria than to any other disease (Carter and Mendis, 2002, Goldsmith, 2010).

Italy's capital, Rome, was reportedly the most malarious large city on Earth – the illness was known as Roman fever or marsh fever. Marshes and swamplands used to cover extensive areas in Italy and each summer the yearly flooding of the Tiber river brought back the illness with a vengeance (Goldsmith, 2010). The receding river left pools of stagnant water behind, which provided the perfect breeding ground for the anopheles mosquito – the vector of the human malaria parasite. The Romans, oblivious to the fact that mosquitoes carry malaria, thought the disease came from the foul-smelling gases – caused by rotting dead animals and plants – that drifted into the villages and towns from the swamps. The Romans called the gases *mal aria*, which means "bad air" and that's how marsh fever became known as malaria (Goldsmith, 2010).

Until the mid-1800's, malaria was a complex puzzle that scientists and doctors didn't know much about. The ultimate breakthrough came in 1880 when Charles-Louis-Alphonse Leveran, a French military physician based in Algeria, observed malaria parasites in the blood of a soldier using a microscope (Goldsmith, 2010, Ariey et al., 2019). By 1890, through the work of other researchers from Italy and the U.S., it was known that a protozoan parasite which multiplied in erythrocytes was the cause of malaria. Four different species of the *Plasmodium* parasite were named and identified as causative agents of malaria in humans; *P. falciparum*, *P. vivax*, *P. ovale* and *P. malariae* (Gaur et al., 2016).

The last piece to the malaria puzzle was figuring out the transmission mechanism of the parasite. This was achieved by Sir Ronald Ross, a British physician, who observed the *Plasmodium* parasite in the stomach of an anopheles mosquito which he dissected four days after feeding on a malaria patient. These discoveries led to the present-day understanding of the malaria life cycle and ultimately the advancements in combating malaria transmissions (Gaur et al, 2016).

2.3 The *Plasmodium* life cycle

Symptoms of malaria can develop as early as six to eight days after an individual is bitten by an infected mosquito, or as late as several months after leaving the area of infection (Tuteja, 2007). Identifying malaria based on symptoms can be challenging as the initial signs are non-specific and can vary. Some of the early symptoms include chills, fever, headache, diarrhoea, abdominal pain, weakness, dizziness, itchiness, lack of appetite, and muscle pain (Tangpukdee et al., 2009). The majority of individuals infected with malaria do not exhibit any or very few symptoms. Nevertheless, the parasite undergoes the same human-parasite interaction and life-cycle morphological transformations (Milner, 2018).

The lifecycle of the malaria parasite in the human host and mosquito vector is illustrated in Fig 2.1. Malaria infection starts when sporozoites, the immature and motile spore-like forms of the *Plasmodium* parasite, are inoculated within a human vein by an infected female anopheles mosquito (Miller et al., 1994). The sporozoites move to the liver through the bloodstream and invade the liver cells (hepatocytes), in which each sporozoite undergoes asexual replication for 9-16 days giving rise to tens of thousands of merozoites. The merozoites are released into the bloodstream where they invade red blood cells (erythrocytes) and multiply to form new merozoites. The infected erythrocytes burst, releasing merozoites that infect new erythrocytes, leading to another cycle of invasion and growth (Gaur et al., 2016). The blood stages of the

plasmodial life cycle causes the pathology and clinical symptoms, such as fever attacks, associated with malaria (Barnes, 2011). The duration between fever attacks is associated with the length of the cycle of invasion. Infection by *P. falciparum*, *P. vivax* and *P. ovale* result in fever attacks occurring every third day (48-hour intervals) while fever episodes for patients infected by *P. malariae* will occur at 72-hour intervals.

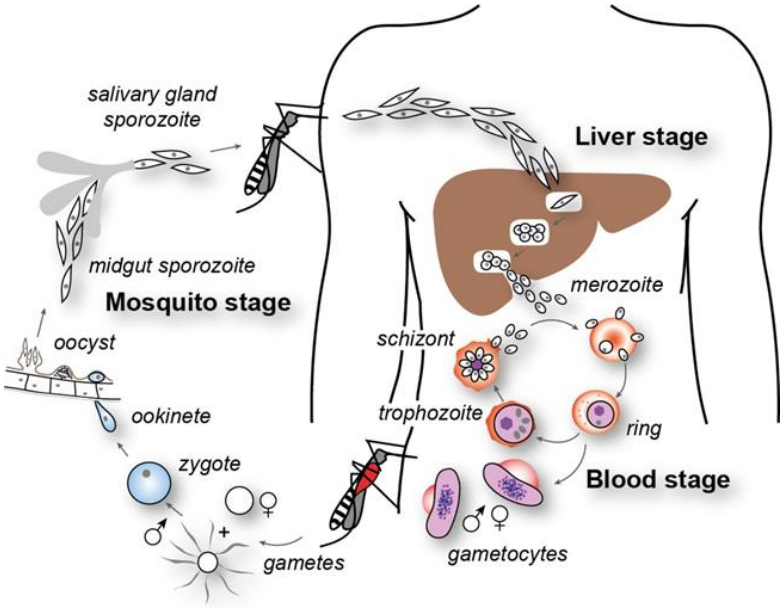

Figure 2.1. The lifecycle of the malaria parasite in the human host and anopheline mosquito vector. (Cowman et al., 2012).

After several cycles, the sexual forms of the parasite (gametocytes) are produced in the erythrocytes instead of merozoites. The gametocytes are ingested by female, i.e. anopheline, mosquitoes during a blood meal. Male and female gametocytes fuse within the gut of the mosquito to form a zygote, elongate and develop into a motile ookinete (Fig. 2.1). It crosses the midgut epithelial lining and forms an oocyst under the mosquito's outer gut lining. Several spindle-shaped sporozoites form through asexual multiplication within the oocyst and migrate to accumulate in the mosquito's salivary glands. The infected mosquito injects these

sporozoites with saliva into the next human host, thereby completing the life cycle (Becker et al., 2010, Gaur et al., 2016).

2.4 Malaria control

Following the discovery of the *Plasmodium* parasite and the role of the anopheles mosquito as vectors, better approaches for malaria control were developed by malariologists. Regional malaria elimination campaigns primarily focused on vector control measures resulting in a substantial decrease in malaria mortality and morbidity in Europe and the Americas at the start of the 20th century were initiated (Tanner and Savigny, 2008). In the early 1940's, dichloro-diphenyl-trichloroethane (DDT) was developed as the first residual contact pesticide to kill indoor-resting mosquitoes. Field trials in homes had spectacular results everywhere, raising optimism at the possibility of malaria eradication. The newly formed World Health Organization (WHO) was given the mandate to launch the Global Malaria Eradication Program (GMEP) at the 8th World Health Assembly (Tanner and Savigny, 2008, Nájera et al., 2011).

The WHO used DDT in combination with remarkably efficient antimalarial drugs, such as chloroquine, to successfully eliminate malaria from the Caribbean, Europe, North America and parts of South-Central America and Asia by the end of the 1960's. However, it was soon realised that short term strategies would not suffice in the quest for malaria eradication, particularly in sub-Saharan Africa. This was due to the wide variability in parasites, vectors, human behaviour, ecology, infrastructure as well as the unsustainable political and economic operational costs of the campaign. The resurgence of malaria transmission across the Western Pacific and southern Asia combined with the spread of insecticide resistance by vectors and drug resistance by parasites resulted in the GMEP being abandoned in 1969 (Nájera et al., 2011, Tanner and Savigny, 2008, Carter and Mendis, 2002, Breman et al., 2000).

The WHO learned important lessons from the successes and failures of the GMEP (1955 – 1969) "malaria eradication" effort. In subsequent decades, anti-malaria campaigns moved from a vertical, disease specific approach to supporting the delivery of a more integrated health service – combining vector control with meticulous malaria case detection and treatment (World Health Organization, 1999, Carter and Mendis, 2002). Studies carried out in the 1990's indicated the possibility of significantly reducing malaria mortality by (1) reducing mosquito bites through widespread use of insecticide-treated materials, (2) early and effective treatment of suspected malaria cases in order to decrease the chances of drug resistance, and (3) rapid and efficient responses to possible malaria epidemics (World Health Organization, 1999, Tanner and Savigny, 2008).

2.4.1 Vector control

Vector control is considered the most effective way of controlling malaria transmission (Najera and Zaim, 2001). It is the only method that has led to long-lasting malaria eradication (Takken and Knols, 2009). The aim of vector control is to both stop transmission by decreasing human-vector contact and reducing the vector population (Ariey et al., 2019). The most successful approach uses a combination of chemical, biological, physical, genetic and environmental management (Ariey et al., 2019). Chemical control by application of insecticides against adult-stage mosquitoes is the most commonly used control tool in the majority of vector control programs across the world (Raghavendra et al., 2011). The core chemical control interventions applicable for populations at risk of malaria are indoor residual spraying (IRS) and insecticide treated nets (ITNs) (World Health Organization, 2019).

2.4.2 Indoor residual spraying (IRS)

Indoor residual spraying with insecticides to kill mosquitoes is the mainstay for large scale malaria control (Raghavendra et al., 2011). It is responsible for greatly reducing malaria incidence during the early twentieth century and eliminating malaria as a public health problem

in Russia, Latin America, Europe and Asia (Pluess et al., 2010, Raghavendra et al., 2011). IRS involves the spraying of long-lasting, residual insecticides onto ceilings and interior walls of homes or structures where adult vector mosquitoes potentially land and rest and subsequently come into contact with the insecticide (World Health Organization 2015a). This reduces the lifespan and the density of female mosquitoes thereby decreasing malaria transmission.

2.4.3 Insecticide treated nets (ITN's)

Bed nets are one of the oldest anti-mosquito measures, simply designed to physically block mosquitoes from biting people sleeping underneath them (Curtis, 1996). The invention of stable synthetic pyrethroids, which exhibited both low toxicity to mammals and high insecticidal activity, enabled the development of insecticide impregnated nets for malaria control (Lengeler et al., 1996, Shiff, 2002). The scent of body odours and carbon dioxide exhaled by humans during sleep serve as attractants for mosquitoes towards the ITNs, which kill or repel mosquitoes upon contact with the insecticides (Killeen et al., 2007). Denying female mosquitoes a blood meal stops egg development and subsequently reduces mosquito population and transmission (Mendis et al., 2009). Since the mid-1990s, ITNs have been recognized as a crucial tool in the fight against malaria, regarded as the most effective control measure since the implementation of IRS and chloroquine. This has made them an essential component of national and global malaria control policies (Hill et al., 2006). Increased ITN coverage in sub-Saharan Africa between 2000 and 2015 was successful in preventing an estimated 68% of the 663 million averted cases due to malaria control strategies (Killeen, 2020, World Health Organization, 2016, World Health Organization, 2015b).

2.4.4 Shortfalls of IRS and ITN's

The principal drawback of IRS and ITN's for malaria vector control is the development of insecticide resistance in mosquitos, specifically pyrethroid resistance. The emergence of resistance to the four classes of insecticides (carbamates, organochlorines, organophosphates

and pyrethroids) most often used in public health has been reported in populations of anopheles *gambiae* in many countries in Africa since the early 2000's (Aïkpon et al., 2014). IRS use has declined since the 1980's as a result of the adverse publicity on the safety and environmental hazards of DDT, as well as the reduction in production and availability of DDT, especially in formulation which meet WHO specifications (Najera and Zaim, 2001).

One potential solution is to replace DDT with a WHO-approved insecticide, such as fipronil, and utilize wall linings that are infused with the insecticide as controlled release devices instead of residual spraying.

2.5 Fipronil

Fipronil is a broad-spectrum, low-application-rate insecticide that belongs to the class of compounds known as phenylpyrazoles (Fig. 2.2) (Gols et al., 2020, Tingle et al., 2003, Gupta and Anadón, 2018, Simon-Delso et al., 2015). This systemic neurotoxin is widely used for controlling pest organisms of animals and crops, e.g. fleas, weevils, ants, ticks, rootworms, mosquitoes, and termites (Jackson et al., 2009). Fipronil and its major metabolite, fipronil sulfone, kill insects by non-competitively binding to the γ-aminobutyric acid (GABA) receptor thereby blocking channels involved in the transmission of neural signals (Moraes et al., 2020, Margarido et al., 2013). Its distinctive mode of action presents a potent alternative for controlling insects that have developed resistance to classical insecticides such as pyrethroids, carbamates, organophosphates and organochlorines (Kumar et al., 2019, Gupta and Anadón, 2018).

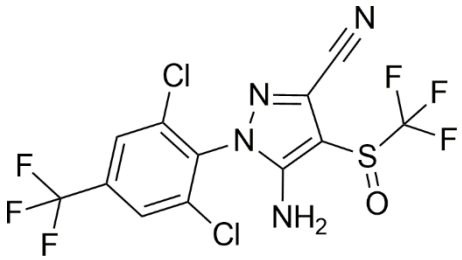

Figure 2.2. Structural formula of 5-amino-1-[2,6-dichloro-4-(trifluoromethyl)phenyl]-4-[(trifluoromethyl)sulfinyl]-1H-pyrazole-3-carbonitrile (fipronil).

According to patents (Saxell et al., 2018, Saxell et al., 2014, Saxell et al., 2013, Saxell et al., 2011, Zamir, 2013, Zamir, 2015) and open literature (Park et al., 2017), fipronil can crystallize in several different polymorphic/pseudo-polymorphic forms. These forms were characterized by powder X-ray diffraction (PXRD), infrared spectroscopy (IR), differential scanning calorimetry (DSC) and thermogravimetric analysis (TGA) by these authors. Saxell *et al.* reported four polymorphs of fipronil which they named crystalline modifications CM-I (Saxell et al., 2013), CM-II (Saxell et al., 2011), CM-IV (Saxell et al., 2014) and CM-V (Saxell et al., 2018). Crystalline modifications CM-I and CM-V were identified to be the thermodynamically stable forms with melting temperatures corresponding to 196 °C and 203 °C, respectively. The crystalline modifications CM-II and CM-IV were identified to be solvates of their corresponding co-crystallized solvents. The removal of the co-crystallized solvent in crystalline modifications CM-II and CM-IV resulted in endothermic phase transformations leading to crystalline modifications CM-I and CM-V and/or mixtures of them. Table 2.1 summarises some of the characteristics of the fipronil modifications reported by Saxell *et al*. (Saxell et al., 2014, Saxell et al., 2011, Saxell et al., 2018, Saxell et al., 2013).

Table 2.1. Single crystal data and DSC information for fipronil polymorphs reported in literature.

Crystalline modification	Crystal system Space group*	Unit cell parameters	DSC event# (°C)	Reference
CM-I	monoclinic *C*2/*c*	*a* - 22.2462 Å *b* - 12.7041 Å *c* - 14.6262 Å α - 90° *β* -128.8891° *γ* - 90° Z = 8 ρ - 1.81 g·cm^{-3}	m.p. 196 – 198↓ T_p = 196	(Saxell et al., 2013)
CM-II	monoclinic $P2_1/c$	*a* - 8.6061 Å *b* - 26.9192 Å *c* - 16.0861 Å α - 90° *β* - 102.0661° γ - 90° Z = 4 ρ - 0.94 g·cm^{-3}	130↓ 196↓, 203↓	(Saxell et al., 2011)
CM-IV	triclinic *P*-$\bar{1}$	*a* - 8.6461 Å *b* - 13.0931 Å *c* - 16.6862 Å *α* - 99.2021° *β* -103.2251° *γ* - 99.5691° Z = 2 ρ - 1.64 g·cm^{-3}	128↓ 196↓, 203↓	(Saxell et al., 2014)
CM-V	triclinic *P*-$\bar{1}$	*a* - 8.6764 Å *b* - 9.1644 Å *c* - 11.3674 Å α - 90° β - 87.2168° γ - 83.4508° Z = 2 ρ - 1.73 g·cm^{-3}	m.p. 201 – 204 203↓	(Saxell et al., 2018)
	monoclinic *C*2/*c*	*a* – 22.564916 Å *b* – 12.68239 Å *c* – 14.905111 Å β – 129.6993° Z = 8		(Park et al., 2017)
	monoclinic $P2_1/n$	*a* – 10.78018 Å *b* – 12.70069 Å *c* – 12.10399 Å β – 96.9731° Z = 4 ρ - 1.701 g·cm^{-3}		(Tang et al., 2005)

*: *a*, *b*, *c* are the lengths of the unit cell edges; α, β, γ are the angles of the unit cell, Z represents the number of asymmetric units in the unit cell and ρ is the calculated density.
#: ↓ denotes an endothermic eventT_p: the peak temperature

Zamir (Zamir, 2015, Zamir, 2013) reported five polymorphs of fipronil which were named Form F-I, F-II, F-III, FS-T and FS-M. The DSC curve of Form F-I featured a single dominant endotherm ascribed to melting, centred at 202.5 °C, while the curve for Form F-II featured a second endotherm at *ca*. 195 °C. The melting points reported for Form F-I and F-II are similar to those reported by Saxell *et al.* for crystalline modification CM-V (Saxell et al., 2018) and CM-I (Saxell et al., 2013), respectively. Fortunately, both patent data sets reported PXRD patterns for the different polymorphs which they identified. Perusal of these diffractograms indicated a correspondence between F-I and CM-V as well as between F-II and CM-I. Crystal modifications CM-IV and Form F-III do not have corresponding polymorphs listed in the two separate sets of patents. FS-T and FS-M were considered hemi-solvates. They contained co-crystallized toluene and methyl isobutyl ketone (MIBK) respectively. The removal of the co-crystallized toluene from FS-T by heating the sample in a DSC resulted in an endothermic phase transformation of FS-T to Form F-III at *ca*. 110 °C. Upon heating, Form F-III underwent an exothermic transformation to Form I at 150 °C.

Beyond these studies, Park et al. (2017) and Tang et al. (2005) reported single crystal XRD data. The sample studied by the former was obtained by slow evaporation from an acetonitrile solution at room temperature. The unit cell parameters reported by both these investigators are also reported in Table 2.1.

On comparing the results reported in all of these studies, it is clear that there is a lack of consensus on the actual crystal structure of the solvent-free polymorphs. Also, the two melting points seen in the DSC curve of a purportedly pure polymorph, Form F-II (Zamir, 2015), poses a further conundrum. Therefore, the aim of this work was to bring greater clarity to the situation by a detailed investigation of the polymorphic behaviour of fipronil using DSC, PXRD, SCXRD and HSM as complementary investigative tools. Solvate and pseudopolymorph characterization was investigated using TGA.

2.6 Polymorphism

A comprehensive definition of crystal polymorphism is elusive in the field of chemistry. The term *polymorph* was first defined in 1965 by Walter C. McCrone as "*a solid crystalline phase of a given compound resulting from the possibility of at least two different arrangements of the molecules of that compound in the solid state*" (Davey, 2002). McCrone's "universal" criterion for polymorphic classification further states that polymorphs may have different crystal structures but lead to identical liquid and vapour states (Dunitz and Bernstein, 1995, Davey, 2002). A statistical evaluation of the frequency of polymorphism by Grunenberg (1997) established that nearly 80% of the organic substances existed as polymorphs, pseudo-polymorphs (solvates) or amorphous forms. This implied that polymorphism was the rule rather than the exception (Olenik and Thielking, 2012).

Seven fundamental crystalline systems exist in which the atoms of a molecule may be arranged in the solid state. These are monoclinic, triclinic, trigonal, tetragonal, hexagonal, cubic or orthorhombic systems (Giron, 1995). Some crystalline compounds may react with the solvent or moisture in the air to form distinct solid phases known as "solvates" and "hydrates", respectively. These phases are often referred to as "pseudo-polymorphs" (Giron, 1995). Due to the different physicochemical characteristics, polymorphs and pseudo-polymorphs may vary greatly in their physical properties such as melting and sublimation temperatures, density, hardness, heat capacity, crystal shape, colour, solubility, as well as in their electrical and optical properties (Dunitz and Bernstein, 1995, Giron, 1995).

2.6.1. Detection of polymorphism

Polymorphs can be distinguished by the differences in their physical properties. The most effective methods used to study polymorphism are: (i) thermogravimetric analysis (TGA); (ii) differential scanning calorimetry (DSC); (iii) polarization thermal microscopy; (iv) thermo-optical analysis (TOA); (v) powder X-ray diffraction (PXRD); (vi) solubility and (vii) infrared

spectroscopy (FTIR) (Perrenot and Widmann, 1994). Thermal analysis and combined techniques such as heat controlled X-ray diffractometry and heat controlled FTIR make analysis of thermodynamic relationships easier (Giron, 1995).

2.6.2. Thermodynamic and kinetic aspects of polymorphism

Crystallization in polymorphic systems is governed by a combination of kinetic and thermodynamic factors (Bernstein et al., 1999). If we consider two polymorphic solids, their relative stability depends on their Gibbs free energies according to the Gibbs–Helmholtz-equation (Equation (1)), which relates the Gibbs free energy (*G*) and the enthalpy (*H*) to the absolute temperature (*T*) and entropy (*S*) (Bernstein et al., 1999, Grunenberg et al., 1996, Olenik and Thielking, 2012):

$$G = H - TS \qquad (1)$$

The system desires to minimize its Gibbs free energy, hence, the polymorph with lower Gibbs free energy will be the most stable form and should consequently be preferred during crystallization (Bernstein et al., 1999, Olenik and Thielking, 2012). With the exception of transition points, where the Gibbs free energies of polymorphs are equal, only one polymorph has the lowest Gibbs free energy under a defined set of experimental conditions. This polymorph is called the thermodynamically stable form while the other polymorph(s) are known as metastable form(s) (Lohani and Grant, 2006).

Polymorphic transformations can be grouped into two transition states – enantiotropic and monotropic phase transitions (Olenik and Thielking, 2012). Enantiotropic transitions between two polymorphs occur reversibly without passing the liquid or gaseous phases, while monotropic transitions are irreversible (Grunenberg et al., 1996, Giron, 1995). An enantiotropic relationship implies that the lower melting form is the thermodynamically stable form at temperatures below the transition point while the higher melting form is the thermodynamically

stable form at temperatures above the transition point. In the case of monotropy, one form is metastable with respect to the other at all temperatures (Giron, 1995, Threlfall, 1995).

The Gibbs free energy (*G*) and enthalpy (*H*) are functions of temperature (*T*) at constant pressure and the variation in Gibbs free energy between the dimorphic system (i.e. a mixture of two polymorphs) and the melt (liquid) may be presented graphically in an energy vs temperature diagram (Grunenberg et al., 1996). Diagrams based on the variation of Gibbs free energy with temperature for a polymorphic system contain an abundance of information in a compact form, and give a visual and readily interpretable summary of the generally complex relationships among polymorphs (Davey, 2002). A typical Gibbs free energy vs temperature diagram is given in Fig. 2.3. It is made up of *G*- and *H*-isobars of the two crystalline polymorphs and of the liquid phase (the melt). The diagram is an illustration of an enantiotropic system, in which form II is the stable form below the transition point.

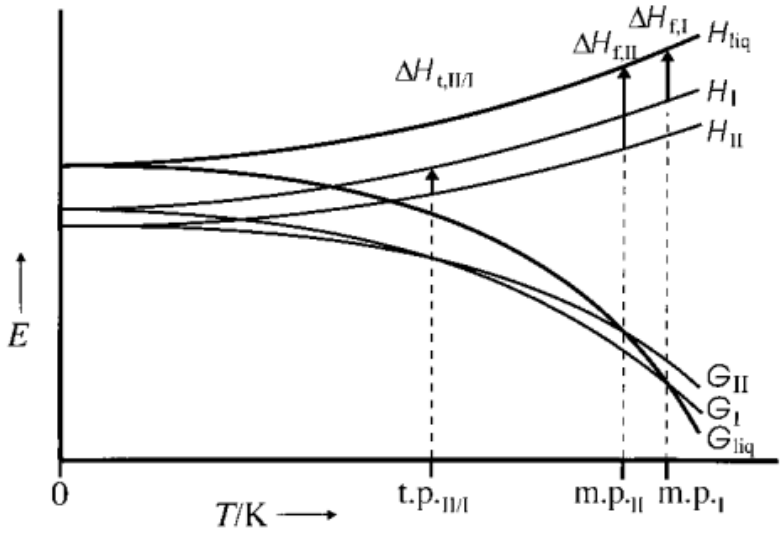

Figure 2.3. Energy versus temperature diagram of an enantiotropic dimorphic system illustrating the variation of the Gibbs free energy (*G*) and enthalpy (*H*) with Temperature (*T*). The Roman numerals indicate the two polymorphs: m.p. is the melting point and t.p.$_{II./I}$ represents the transition point between the two polymorphs (Bernstein et al., 1999). (Reprinted with permission from Wiley.)

Several noteworthy observations can be made from the plot. For example, the experimental generation of H isobars can be achieved through measurement of the heat capacity from

$$\left(\frac{\partial H}{\partial T}\right)_p = C_p \qquad (2)$$

The fundamental relationship between the enthalpy and the heat capacity, is illustrated in Fig. 2.4.

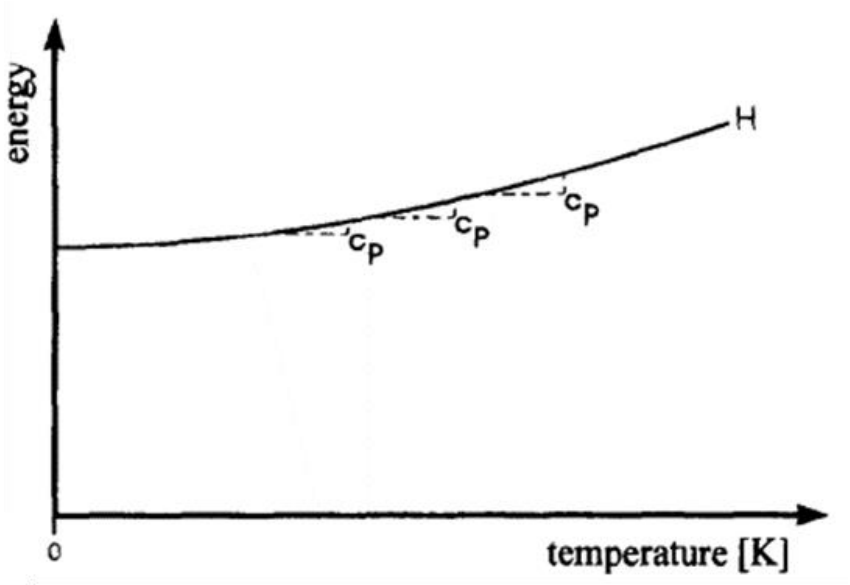

Figure 2.4. Enthalpy vs temperature diagram specifying the relationship with the heat capacity, C_p (Grunenberg et al., 1996) (Reprinted with permission from Elsevier.)

According to the third law of thermodynamics, the heat capacity of a substance should be zero at 0 K (absolute zero), implying that the slope of a curve of enthalpy (*H*) versus temperature (*T*) should be zero at absolute zero (Grunenberg et al., 1996, Klimenko, 2012). As a result, the most stable polymorph should have the lowest Gibbs free energy at absolute zero (Bernstein et al., 1999).

Fig. 2.3 also indicates that the liquid phase of a substance has a higher energy than its crystalline forms at absolute zero (Fig. 2.3), hence the *H*-isobar of the liquid is located above the isobars of the solid polymorphs of the corresponding substance (Grunenberg et al., 1996).

At absolute zero, the *TS* term in Equation 1 will be zero and the Gibbs free energy equals the enthalpy, i.e. $G = H$. Consequently, the *G*- and *H*-isobars of specific polymorphic forms and that of the liquid converge at absolute zero (Grunenberg et al., 1996). Since *S* is invariably positive, *G* is a continuously decreasing function as seen in Fig. 2.3 (Davey, 2002). The exact path of the *G*-isobars cannot be experimentally followed since the entropy cannot be determined. However, solubility data can be used to predict the relative positions of the *G*-isobars (Grunenberg et al., 1996).

The G_I and G_{II} curves in Fig. 2.3 represent the trajectory of Gibbs free energy as a function temperature for two polymorphs. The two Gibbs free energy curves intersect at the thermodynamic transition point $t.p._{II/I}$, but because the enthalpy of I is higher than that of II, the quantity of energy that will be required for the phase transition to occur, indicated by the short black arrow at $t.p._{II/I}$, equals $\Delta H_{t,II/I}$. This energy must be endothermic for a transition above the transition point $t.p._{II/I}$ and exothermic below the transition point $t.p._{II/I}$ for the system depicted in Fig. 2.3. Likewise, $\Delta H_{f,I}$ and $\Delta H_{f,II}$ represent the respective enthalpies of fusion corresponding to the endothermic solid-to-liquid transitions at the melting points (Bernstein et al., 1999).

The solid-solid transition point ($t.p._{II/I}$) in Fig. 2.3 lies at a temperature below the melting points of the two polymorphs and represents an enantiotropic dimorphic system. If the thermodynamic relation between two polymorphs is monotropic, there is no solid-solid transition point below their respective melting points. For this scenario, the Gibbs free energy plotted against temperature will bear a resemblance to the diagram depicted in Fig. 2.5.

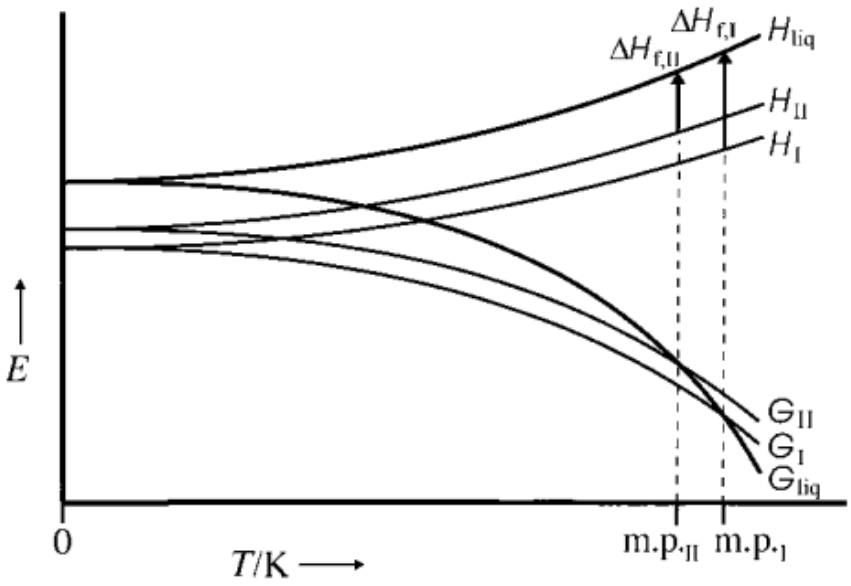

Figure 2.5. The energy vs temperature diagram of a monotropic dimorphic system. All symbols have the same meaning as in Fig. 2.3.

The knowledge of whether a polymorphic relationship is enantiotropic or monotropic can aid in regulating the crystallization procedure to obtain a specific polymorph while excluding the undesired one. If the desired and undesired polymorphs have an enantiotropic relationship, then performing the crystallization at a temperature where the desired polymorph is thermodynamically favoured can promote its crystallization. This can effectively prevent the undesired polymorph from forming and increase the likelihood of obtaining the desired one (Lee, 2014).

2.7 Vapour pressure estimation

Vapour pressure, P, is a measure of the tendency of a substance to enter the gas phase by either sublimation (solid → gas) or evaporation (liquid → gas) (Price, 2001). It influences the volatility of a substance and will, therefore, determine the rate of evaporation from industrial processes or waste sites. Vapour pressure influences the exchange of chemicals across the air-

water interface, and their release into the atmosphere from aquatic systems, soils, and plants. Additionally, vapour pressure controls the adsorption of organic compounds onto airborne particulate matter, with less volatile compounds being preferentially adsorbed. It also affects the removal of particulate matter from the atmosphere by rainfall and dry deposition, as well as the atmospheric residence time of chemicals (Delle Site, 1997, Sonnefeld et al., 1983). Therefore, it is essential to determine the vapour pressures of organic compounds within the ambient temperature range in order to develop environmental transport models and evaluate potential health risks associated with the occurrence of toxic substances atmosphere.

John Dalton (1766-1894) conducted the earliest acceptable vapour pressure measurements by utilizing a barometer enclosed in water and filled with the substance under investigation, while measuring the descent of a mercury column (Wisniak, 2001). Since then, many methods have been described in the literature for the measurement of vapour pressure. However, no single method is applicable for the entire vapour pressure range of environmentally significant compounds (10^5 to 10^6 Pa) (Sonnefeld et al., 1983). The methods used for environmental contaminants are classified into “direct experimental”, “indirect experimental” and “prediction” methods (Delle Site, 1997). In this study, a prediction method was used and reviewed.

The availability of vapour pressure data for chemicals of environmental concern, particularly those with low vapour pressures (<1.0 Pa), is often limited due to analytical difficulties. Additionally, chemical products frequently consist of numerous components, making it difficult to determine the vapour pressures of each component in the mixture, particularly when they are not accessible in their pure state. Prediction techniques, in such situations, may provide an advantageous approach to estimate vapour pressures (Delle Site, 1997).

Knowledge of the chemical and physical properties of insecticides is essential for reliable environmental fate and risk assessments and the subsequent design of effective mitigation and remediation strategies (Singh et al., 2017). The vapour pressure is among the most important physical properties because it plays an important role in governing the gas-phase concentration of pesticides and their stability during long distance transport (Goel et al., 2007).

The TGA method is a useful tool for obtaining estimates of the vapour pressure of organic compounds. Compared to conventional methods of vapour pressure measurement, its advantages include the simplicity of the experimental set-up, short experimental times and that small amounts of the compound are required for analysis (Pieterse and Focke, 2003, Beverley et al., 1999, Rong et al., 2012, Parker and Babas, 2014). Initial TGA-based vapour pressure studies (Price, 2001, Phang and Dollimore, 2001) based the TGA data analysis on Langmuir evaporation (Langmuir, 1913). However, the Langmuir model is strictly valid for volatilisation into a vacuum. Therefore, it can only be used to predict the vapour pressure from TGA mass loss measurements conducted at vacuum conditions (Szczotok et al., 2019, Pieterse and Focke, 2003).

TGA mass loss measurements in the dynamic mode are usually performed at finite pressures with a flow of gas that controls the atmosphere. The space above the sample is filled with the purge gas as well as some of the volatilising compound present. The mean free path, i.e. the average distance over which a gas molecule travels between successive collisions with other molecules is very small. At ambient conditions in air, it is only about 66 nm (Jennings, 1988). Furthermore, according to the kinetic theory of gases, the root means square velocity is given by the equation:

$$v_{rms} = \sqrt{3RT/M} \qquad (3)$$

With nitrogen as the gas, this velocity is predicted to be about 23 $m \cdot s^{-1}$, i.e. very fast. The implication is that the evolved sample molecules are subjected to heavy pummelling by the nitrogen gas molecules as they travel upwards to escape from the open-top crucible. This means that the rate of migration of an evaporating sample molecule through the gas trapped inside the crucible is much lower than the maximum rate possible as predicted by the Langmuir equation. Therefore, diffusion effects must be considered when attempting to estimate vapour pressures from TGA mass loss rates.

In the gravimetric method for the determination of liquid evaporation rates, the sample is held in a partially filled, cylindrical open-ended crucible. Analytical solutions, appropriate to this geometry, can be derived. They can account for the variation of the evaporation rate with liquid depth within the sample crucible and the vapour diffusion coefficient for the evaporating compound in the purge gas. Two different gas flow configurations are possible as shown in Fig. 2.6(a) and 2.6(b).

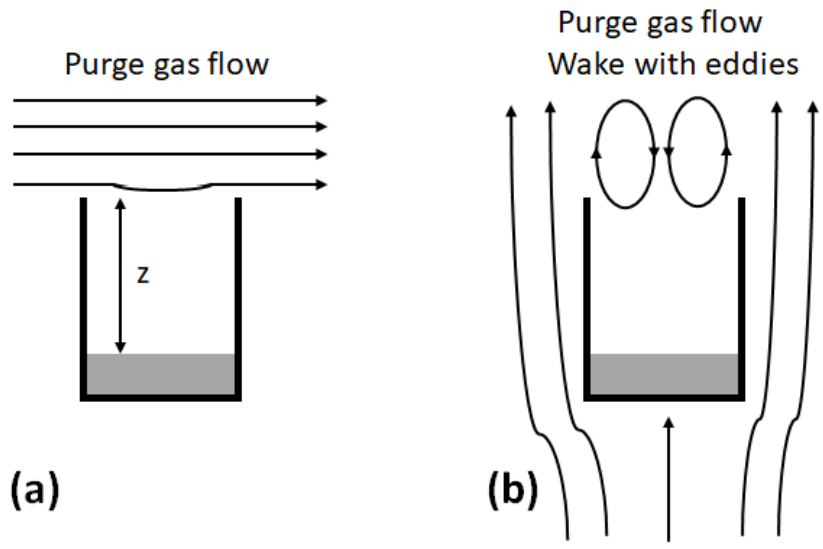

Figure 2.6. (a) Cross- and (b) axial gas flow configurations used for measuring the sublimation and evaporation rates of compounds in the TGA apparatus.

Pieterse and Focke (2003) analysed the case in which the gas flows across the top of the crucible as shown in Fig. 2.6(a). In Fig. 2.6(b) the gas flow is in an axial upward direction past the cylindrical crucible. This latter case was first analysed by Beverley et al. (1999). The streamlines defining the gas flow are also shown schematically in Fig. 2.6. In both cases, the passing gas stream induces secondary flow patterns at the top entrance to the crucible. Depending on the flow rate, these may even take the form of vortices or eddies as shown in Fig. 2.6(b). This means that the gas column inside the crucible is not necessarily quiescent. Furthermore, it implies that the actual diffusion path length is not well-defined. The physical models used to describe the evaporation from the open cylindrical containers fail to adequately consider these effects. Nevertheless, it is possible to reduce these effects by precisely regulating the gas flow rate as suggested by Pieterse and Focke (2003). Nonetheless, Parker and Babas (2014) as well as Rong et al. (2012) developed amendments for the cross-flow (Fig. 2.6(a)) and the axial flow (Fig. 2.6(b)) configurations respectively.

Goel et al. (2007) determined the vapour pressure-temperature relationships for fipronil, in the sub-cooled liquid state, using a gas chromatographic retention time technique. They reported data up to a temperature of 45 °C. The estimates indicated that fipronil does not readily volatilize and will not likely be found in the air.

Chapter 3

Materials and Methods

3.1 Introduction

This chapter gives a description of the chemicals, the experimental methods and analytical techniques applied in order to achieve the objectives of this study.

The first section of the chapter describes the methodology followed to examine the thermal properties of fipronil with specific focus on its sublimation/evaporation behaviour. Firstly, dynamic TGA and DSC runs were carried out to determine the mass loss behaviour and phase transitions over the temperature range of interest. Thereafter, the optimum flow rate for carrying out the sublimation studies was determined by isothermal TGA experiments, using N_2 as carrier gas. Finally, the vaporization rates of a suitable standard (benzoic acid) and fipronil were measured by isothermal TGA at the optimum N_2 flow rate and the results were used to estimate the enthalpies of sublimation and vaporization.

The second part of the chapter describes the methods used to obtain different crystal forms of fipronil by recrystallizing the as-received neat fipronil from acetone, acetonitrile, ethyl acetate and methanol. The neat fipronil and the different crystal forms were analysed by TGA, DSC, hot stage microscopy, PXRD and SCXRD.

3.2 Sublimation characterization and vapour pressure estimation of fipronil using Thermogravimetric analysis

3.2.1. Materials

5-amino-1-[2,6-dichloro-4-(trifluoromethyl)phenyl]-4-[(trifluoromethyl)sulfinyl]-1H-pyrazole-3-carbonitrile (fipronil, 96% purity) was supplied by Avima, South Africa. Reagent

grade benzoic acid (≥99.5%) was purchased from Sigma Aldrich (South Africa). All the chemicals were used without further purification.

3.2.2 Equipment

Mass loss determinations were carried out using a SDT Q600 (TA Instruments) with a horizontal furnace with gas flow as in Fig 2.6(a). A multipoint temperature calibration was performed using indium, zinc and gold calibration standards. Mass calibration was carried out using the manufacturer supplied mass calibration set. The measurements were carried out in dynamic nitrogen (N_2) atmosphere.

3.2.3 Non-isothermal TGA and DSC measurements

A sample mass of approximately 5 mg placed in an open 90 µL alumina crucible in order to minimize thermal gradients but sufficient to fully cover the bottom of the crucible. A dynamic TGA temperature scan, from ambient to 300 °C, was performed on fipronil. The heating rate was 1 °C min^{-1} with nitrogen flowing at a rate of 120 mL min^{-1}. The purpose of the run was to identify the location of the mass loss steps and the temperature where the mass loss rate reached a plateau. The DSC curve was used to identify phase transitions associated with mass loss events.

3.2.4 Determination of optimum flow rate

Isothermal TGA experiments were conducted at 190 °C. The furnace temperature was programmed to increase at a linear heating rate of 10 °C min^{-1} from ambient to the target temperature and then kept in isotherm. The N_2 gas flow rate was varied from 60 to 160 mL min^{-1} in order to identify the optimum condition for the sublimation studies.

3.2.5 Determination of sublimation/evaporation rates and the vapour pressure from TGA mass loss curves

The sublimation or evaporation rates (*dm/dt*) and the vapour pressure of fipronil were determined using isothermal TGA in the temperature range 150 to 220 °C. A constant N_2 gas flow rate of 120 mL min^{-1} was used during these experiments. The furnace temperature was programmed to increase at a linear heating rate of 10 °C min^{-1} from ambient to the target temperature and then kept in isotherm. Mass loss rates were determined from a region where the temperature was constant, and the mass loss rate varied linearly with time.

Similar experiments were conducted using benzoic acid as a reference standard in order to validate the method employed for vapour pressure estimation by TGA. The same method and instrumental configuration used for fipronil was applied except that the isothermal sublimation rates of benzoic acid were studied over a temperature range of 40 °C to 70 °C.

3.3 Characterizing the thermal phase behaviour of fipronil

3.3.1 Materials

The suppliers and some of the physical properties of the chemicals used in this study are listed in Table 3.1.

Table 3.1. List of chemicals, selected physical properties and suppliers.

Chemical	MW ($g\ mol^{-1}$)	ρ ($g\ cm^{-3}$)	T_b (°C)	T_m (°C)	Purity (%)	Supplier
Acetone	58.08	0.79 (25 °C)	56	-94	≥99.5	Sigma-Aldrich
Acetonitrile	41.05	0.78 (25 °C)	81.6	-43.8	≥99.5	Ace Chemicals
Benzoic acid	120.12	1.27 (15 °C)	249 (lit.)	121-125 (lit.)	≥99.5	Sigma Aldrich
Ethyl acetate	88.11	0.90 (20 °C)	76.5 – 77.5	84	≥99.5	Sigma-Aldrich
Fipronil	437.15	1.48 – 1.63	510.1	210.1 ± 5 (lit.)	96	Avima
Methanol	32.04	0.79 (20 °C)	64.7	-98	≥99.5	Sigma-Aldrich

3.3.2. Sublimation of fipronil

A portion of the as-received neat fipronil was purified using vacuum sublimation at approximately 180 °C. The vapour was condensed as purified compound on a cold finger and collected for analysis.

3.3.3. Recrystallization of fipronil

Approximately 50 mg of fipronil was dissolved in 4 mL of solvent (acetone, acetonitrile, ethyl acetate or methanol) in a glass vial. The solution was stirred until the fipronil completely dissolved after which the solution was left open to air at room temperature (ca. 23 °C) to allow for evaporation of the solvent until crystallization. The process took 12 to 36 hours. Regular inspection of the crystals allowed for the identification of the best time to harvest crystals.

Single crystals with suitable size were collected and analysed using single crystal X-ray diffraction (SCXRD). The remaining samples were homogenized into a powder and analysed by powder X-ray diffraction (PXRD), thermogravimetric analysis (TGA) and differential scanning calorimetry (DSC). The samples were then heat treated at either 110 °C or 150 °C to drive off any co-crystallized solvent and analysed by PXRD, TGA and DSC.

3.3.4. Single Crystal X-Ray Diffraction (SCXRD) Analysis

X-ray diffraction data of all single crystals were collected at 150.0(2) K using monochromatic Cu-Kα radiation (λ = 1.54184 Å) on a Rigaku XtaLAB Synergy R diffractometer with a rotating-anode X-ray source and a HyPix CCD detector. Data integration, reduction and multi-scan absorption corrections were performed using the CrysAlisPro (Version 1.171.40.23a) software package (Rigaku, 2018). The crystal structures were solved by direct methods or by intrinsic phasing using SHELXT-2013 (Sheldrick, 2015), as part of the WinGX suite (Farrugia, 2012). Structure refinements were done using SHELXL (Sheldrick, 2015) in WinGX (Farrugia,

2012) as GUI. Graphics and publication material were generated using Mercury 3.5 (Macrae et al., 2006).

3.3.5. Thermogravimetric Analysis (TGA)

Thermogravimetric analysis was performed on a TA Instruments Q600 SDT. A multipoint temperature calibration was performed using indium, zinc and gold calibration standards. Mass calibration was carried out using the manufacturer supplied mass calibration set. Approximately 10 mg of sample was placed in a 90 µL alumina open pan and was heated from ambient temperature to 300 °C at a heating rate of 2 °C min^{-1} under a nitrogen atmosphere, controlled at a flow rate of 50 mL min^{-1}. Analyses were performed in duplicate to confirm the observed effects.

3.3.6. Differential Scanning Calorimetry Analysis (DSC)

Differential scanning calorimetry analysis was performed on a Mettler Toledo DSC 1. Temperature calibration was performed using indium and zinc calibration standards. Approximately 8 mg of sample was enclosed in 40 µL aluminium pans with pinhole lids. The temperature was scanned from 25 °C to 300 °C at a heating rate of 5 °C min^{-1}. Nitrogen flow was controlled at a rate of 50 mL min^{-1}.

Heat-cool-heat analysis was carried out by heating the samples at 5 °C/min up to 200 °C, a temperature that is just after the first endothermic peak but before the second endotherm. The samples were immediately cooled to 100 °C at a rate of 5 °C/min and then reheated to 300 °C. The same procedure was repeated but with the first heating going up to 208 °C, a temperature just after the second endotherm.

3.3.7. Powder X-Ray Diffraction (PXRD) analysis

The fipronil samples were characterized using powder X-ray Diffraction (PXRD). The PXRD patterns were collected from 5° to 90° on a PANalyticalX'Pert Pro powder diffractometer with

X'Celerator detector and variable divergence and fixed receiving slits with Fe-filtered Co-Kα radiation. However, the results are reported reflecting 2θ as expected for Cu-Kα radiation.

3.3.8. Hot Stage Microscopy (HSM)

HSM was performed on a Linkam Scientific CSS450 heating stage fitted with a Leica DM2500M optical microscope. About 1-2 mg of the sample was heated at 5 °C min^{-1} up to 150 °C and then at 2 °C min^{-1} from 150 to 200 °C.

Chapter 4

Sublimation characterization and vapour pressure estimation of fipronil using isothermal thermogravimetric analysis

4.1 Introduction

The results of thermal characterization of neat, as-received fipronil are presented and discussed in this chapter. The focus was on studying the thermal properties of fipronil and its sublimation and evaporation behaviour at temperatures commonly encountered during the conversion processes used to prepare polyethylene-based films and films containing fipronil as the contact insecticide. The sublimation and vaporization enthalpies were determined from isothermal TGA data. This part of the investigation sheds light on the fundamental characteristics of fipronil, which can inform its applications in various fields.

4.2 Non-isothermal TGA and DSC measurements

The TGA and DSC curves obtained in dynamic mode of heating for fipronil are presented in Fig. 4.1, depicting mass versus temperature (TGA, Figs. 4.1a and b), rate of mass change (*dm/dt*) versus temperature (DTG, Fig 4.1a), and heat flow versus temperature (DSC, Fig. 4.1b).

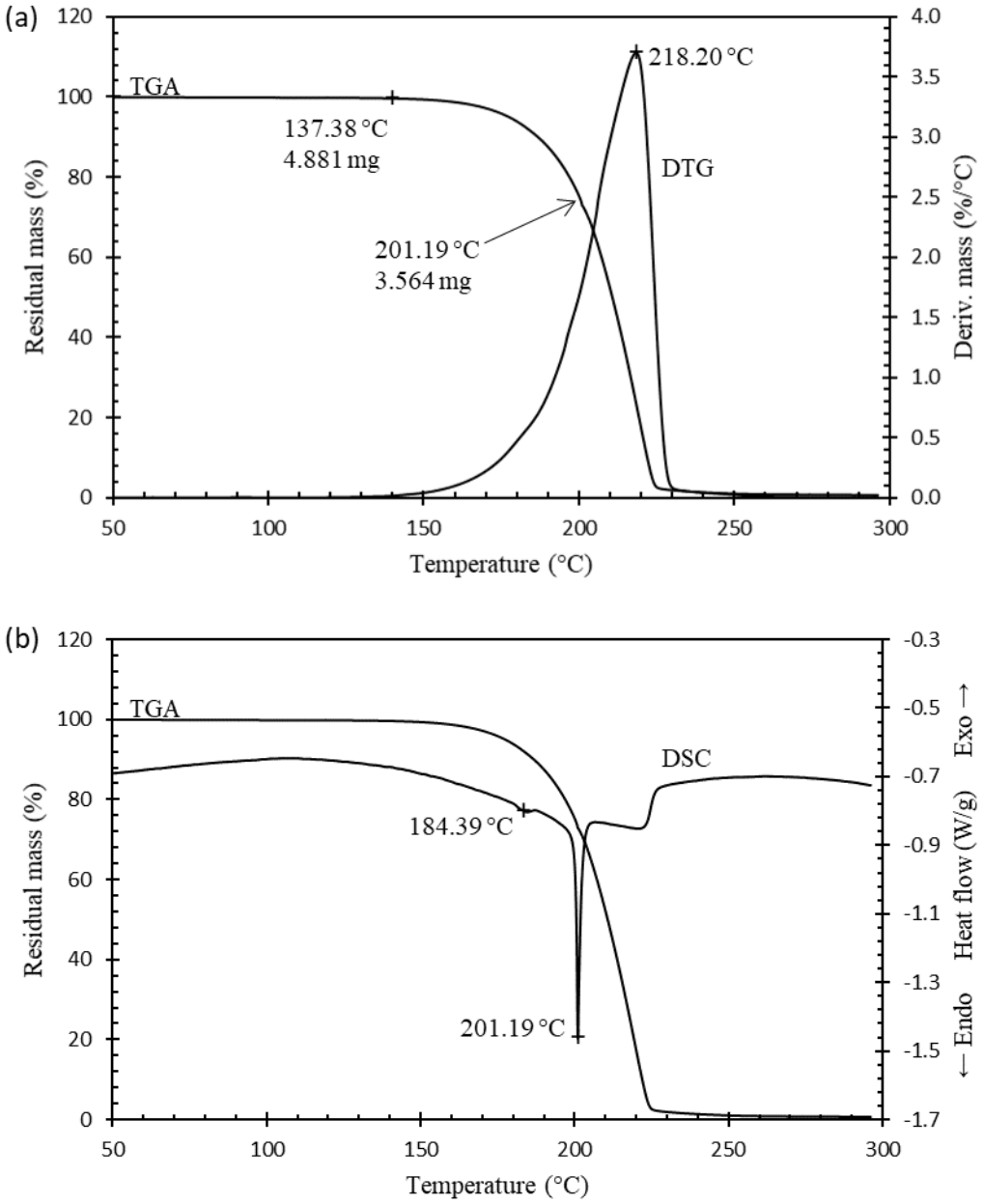

Figure 4.1. (a) TGA and DTG curves and (b) TGA and DSC curves of fipronil when heated linearly at a rate of 1 °C min^{-1} from ambient to 300 °C.

The mass loss of fipronil started at approximately 140 °C and occurred in a single step, resulting in nearly complete mass loss by 260 °C (Fig. 4.1a). The DSC curve displayed three distinct endothermic events (Fig. 4.1b). The first event, starting at approximately 140 °C, appeared as a broad trough that deepened with increasing temperature before abruptly returning to the

baseline above 220 °C. This observed trend was consistent with, initially, the sublimation of the solid and the eventual evaporation of the molten fipronil occurring over a wide temperature range (*ca*. 140-220 °C). The deepening of the trough indicated an accelerated volatilization as the temperature was increased. The small endothermic event located around 185 °C was attributed to an enantiotropic solid-solid phase transition of fipronil. Fipronil is known to exist in at least four different polymorphic and pseudo-polymorphic forms according to patent (Zamir, 2013, Saxell et al., 2014) and open literature (Park et al., 2017) sources. According to Saxell et al. (2011), fipronil melts within the temperature range of 195 to 203 °. Therefore, the sharp endothermic peak at 201.2 °C corresponds to the melting of solid fipronil still present at this temperature. A noteworthy observation is that the mass loss of the sample commenced at a temperature lower than the melting temperature, as shown in Fig. 4.1a. Furthermore, it was observed that only 72.8% of the initial sample amount remained at the onset of melting, which suggests the occurrence of a sublimation process from *ca.* 140 °C preceding the melting. In the TGA plot of fipronil, a sublimation kink, indicated by the arrow in Fig. 4.1a, was detected, resembling a phenomenon observed in a study by Wright et al. (2002) on the thermal properties of benzoic acid. The sublimation process of fipronil was considered to occur from the onset of mass loss to the sublimation kink on the TGA plot, which roughly aligned with the melting point peak on the DSC plot.

Based on these results, the working temperature range for the determination of the enthalpy and entropy of sublimation (and vapour pressure) via isothermal TGA measurements was selected between 150-190 °C to ensure the data used represented the sublimation process. As shown in Fig. 4.1a, there was no sample material left in the crucible beyond 240 °C, as observed by the absence of any residual mass. This indicated that fipronil undergoes melting and complete evaporation upon thermal treatment. The working temperature range for the

vaporization determinations was selected between 195–220 °C to ensure that the data used represent the evaporation process.

4.3 Determination of the optimum flow rate

The flow rate of the purge gas employed in TGA analysis impacts the migration rate of sample molecules evaporating from an open-top crucible, therefore precise control of the gas flow rate is crucial in obtaining an accurate estimation of vapour pressure from TGA mass loss rates. To ascertain the suitable range of flow rates required to achieve a sufficient sublimation rate to saturate the carrier gas, isothermal TGA experiments were conducted.

4.3.1 Determination of optimum flow rate using the Ideal Gas Law

Dalton's law of partial pressure for ideal gas mixtures can be used to calculate the apparent vapour pressure, p' (mPa), when a mass loss, W (g), of a sample at an isothermal temperature, T (K), is caused by a flow rate, V_c (mL min^{-1}), using the equation:

$$p' = \frac{WRT}{MV_c} \qquad (1)$$

where M (g mol^{-1}) is the molar mass of the sample.

In order to establish that the measured values of p'represent the equilibrium vapour pressure data at a given isothermal temperature, it is crucial to observe a chair-shaped curve in the plot of p'against flow rate (Premkumar et al., 2004). Fig. 4.2 displays such a plot for fipronil, calculated from experimental data obtained at an isothermal temperature of 190 °C (463 K). The presence of the plateau within the flow rates range of 100-140 mL min^{-1} demonstrates that the sublimation rate was sufficient to saturate the carrier gas at any flow rate within this range. The midpoint in the plateau, located at 120 mL min^{-1}, was determined to be the optimal flow rate based on this method.

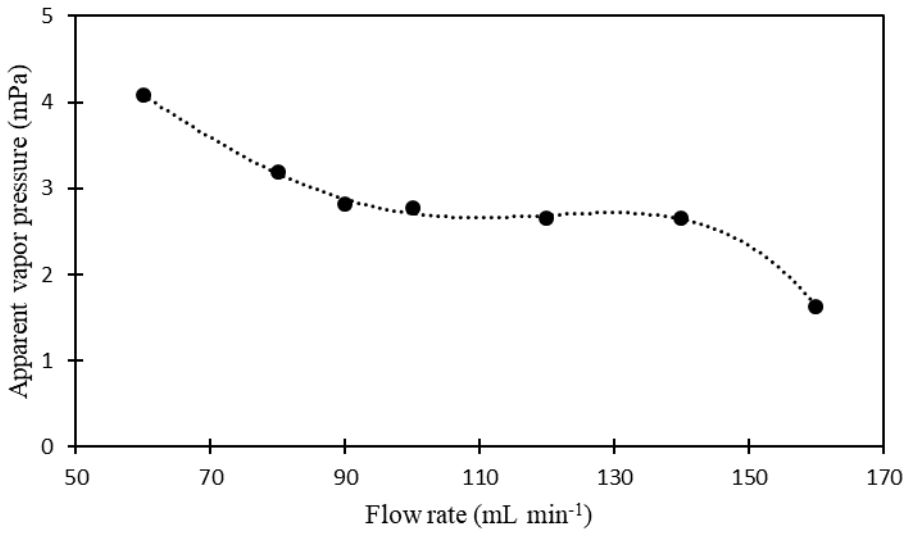

Figure 4.2. Variation of apparent VP of fipronil as a function of flow rate of the carrier gas at 463 K.

4.3.2 Determination of the optimum flow rate using gas permeability

An alternate method for the determination of the optimum flow rate took into consideration the purge gas flow configuration of the TGA. The TGA set-up employed in this study comprised a cylindrical sample cup with an inert gas sweeping over the top as shown in Fig. 2.6(a). In this set-up, the rate of evaporation is controlled by diffusion through the stagnant gas layer above the sample. According to Pieterse and Focke (2003), the rate of vaporisation is given by Equation (2):

$$S_{AB} = P_{AB}D_{AB} = \frac{zRT}{M_A A}\frac{dm_A}{dt} \qquad (2)$$

where dm_A/dt is the TGA-measured mass loss rate (i.e. sublimation/evaporation rate) in g s^{-1}. The mass loss rates were determined from a region where the temperature was constant, and the mass loss rate varied linearly with time. S_{AB} is the nitrogen permeability of the evaporating substance in Pa m^2 s^{-1}; P_{AB} (Pa) is the sample vapour pressure at absolute temperature T (K); R = 8.3145 J $mol^{-1}K^{-1}$ is the gas constant; D_{AB} (m^2 s^{-1}) is the diffusion coefficient; M_A (g mol^{-1})

is the molar mass of fipronil (437.15 g mol^{-1}); A (m^2) is the cross-sectional surface area of the sample cup, and z (m) the depth of the gas-filled part of the sample cup.

The diffusion coefficient for the vaporising compound was estimated using the Fuller correlation (Zghal et al., 2018) using the exposition by Poling et al. (2001). The diffusion coefficient is given in Equation (3):

$$D_{AB} = \left[\frac{10^{-7}\sqrt{1/M_A+1/M_B}}{P(\sqrt[3]{V_A}+\sqrt[3]{V_B})^2}\right] T^{1.75} = CT^{1.75} \quad (3)$$

where D_{AB} is the diffusion coefficient in m^{2}s^{-1}; T is the temperature in K; P is the pressure in atm; M_i is the molecular mass of compound i in gmol^{-1}, and V_i is the diffusion volume for compound i in cm^{3}mol^{-1}. The values for nitrogen are M_A = 28.02 gmol^{-1} and V_A = 18.5 cm^{3}mol^{-1}. The values for fipronil were M_B = 437.15 and V_B = 377.41 cm^3 mol^{-1}. The constant C lumps together the system pressure and all the invariant molecular quantities inside the square brackets of Equation (3). The atmospheric pressure, during the time periods in which measurements were made, was essentially 1 atm. This means that the constant C assumed the value 2.345 × 10^{-10} m^{2}s^{-1}K$^{-1.75}$ for fipronil. Combining Equations (2) and (3) yields a function that equals ln P_A, the integrated Clausius-Clapeyron equation, given in Equation (4):

$$lnP_A = ln\left(\frac{S_{AB}}{CT^{1.75}}\right) = a - b/T \quad (4)$$

where the symbols and their units are as for Equation (4); a and b are adjustable constants with $b = \Delta H/R$, where ΔH is the enthalpy of sublimation or vaporisation in J mol^{-1}.

The impact of the gas flow rate on the measured gas permeability (S_{AB}) of fipronil, as calculated using equation 2, is presented in Fig. 4.3. It was observed that the measured values were independent of the flow rate in the range 80 to 160 mL min^{-1}. Based on this outcome, it was decided to perform all further experiments at a flow rate of 120 mL min^{-1}. This flow rate was also used for the TGA runs performed on benzoic acid.

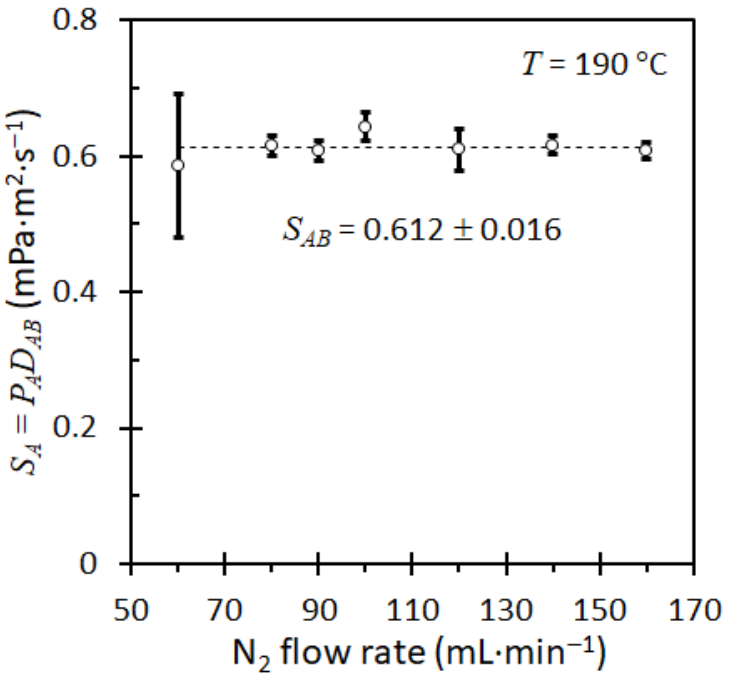

Figure 4.3. Variation of apparent nitrogen gas permeability of fipronil as a function of the flow rate of the carrier gas at 190 °C.

4.4 Vapour pressure estimates for benzoic acid

Benzoic acid is an established calibration standard for thermal analysis techniques (Monte et al., 2006, van Genderen and Oonk, 2003). In order to validate the vapour pressure measurement technique employed, mass loss curves for benzoic acid were recorded in the temperature range 40 °C to 70 °C (Elder, 1997). Fig. 4.4 compares the resulting estimates for the vapour pressure of benzoic acid, calculated using Equation 4, to the reference data reported by Monte et al. (2006).

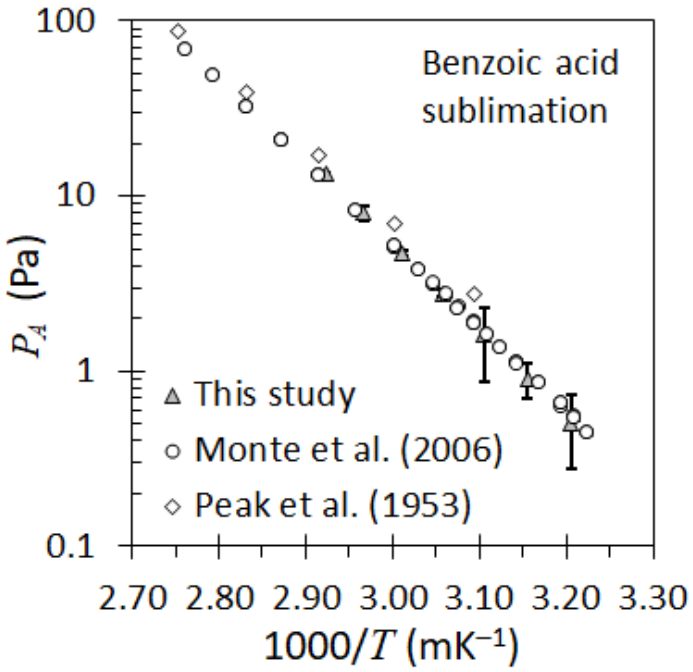

Figure 4.4. Present estimates for the vapour pressure (P_A) of benzoic acid compared to published data (Monte et al., 2006).

The vapour pressure results obtained with the present TGA method are consistent with an enthalpy of sublimation of 97 ± 4 kJ mol^{-1} computed from the Clausius-Clapeyron equation (Equation 4). This is 7.4% higher than the 90.1 kJ mol^{-1} associated with the literature data (Monte et al., 2006). The mean absolute deviation between the present values those of Monte et al. (2006) amounts to 6% with a maximum deviation of 12%. This confirms previous assertions by Pieterse and Focke (2003) regarding the accuracy of vapour pressure measurements attainable with the TGA method. The deficiencies of the TGA method are such that it only provides rough estimates for the vapour pressure of compounds. Nevertheless, the TGA-based estimates results are sufficiently accurate for initial screening experiments, and they are useful for many practical applications.

4.6 Determination of the vapour pressure and enthalpies of sublimation and evaporation

In this section, the vapour pressure and enthalpies of sublimation and evaporation were determined using isothermal TGA.

4.6.1 Determination of sublimation and evaporation rates of fipronil

The rate of fipronil sublimation/evaporation at a given temperature was determined by tracking the rate of mass loss of fipronil by TGA. The method used requires the purity of the sample to be greater than 95% because different components of a mixture cannot be differentiated (Gückel et al., 1995). Being 96% pure with little volatile impurities, the fipronil satisfied the purity requirements.

Fig. 4.5 shows isothermal mode TGA curves in the temperatures between 150 to 220 °C. The vaporisation measurements performed at the lower temperatures continued for a duration of up to 3.5 h. When the temperature was set at 150 °C (curve a), the mass loss rate remained constant over the full measurement period. The cumulative mass loss at the end of the experiment only amounted to 0.35 mg (0.50%). As the applied temperature was increased, the rate of mass loss also increased, leading to termination of the experiments at earlier time points. Specifically, the experiment conducted at 220 °C it was terminated after 30 minutes. The sample exposed to a temperature of 195 °C (curve i) achieved complete mass loss after approximately 2 hours. However, samples heated to higher temperature (≥ 200 °C) did not show complete mass loss. Instead, the formation of a thermally stable residue was evident. This means that the fipronil decomposes at elevated temperatures, forming stable, non-volatile char residues. Interestingly, the amount of stable char formed increased as the imposed isothermal temperature was increased.

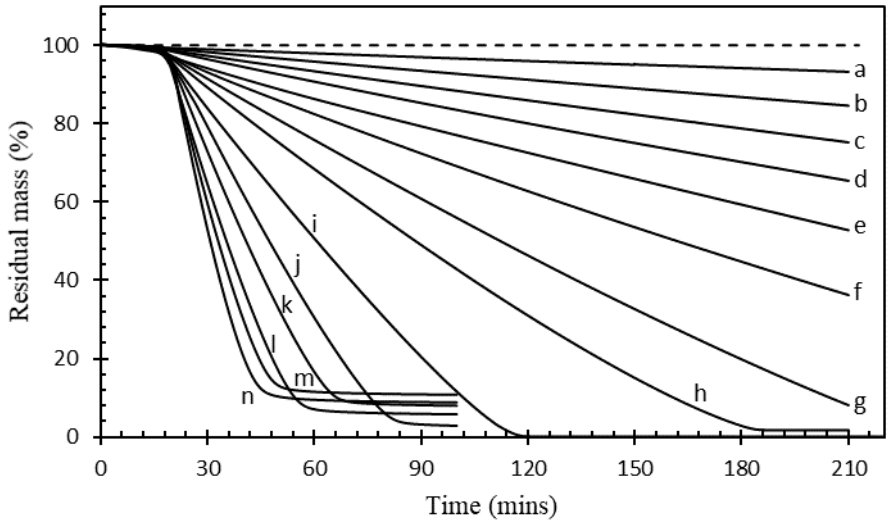

Figure 4.5. TGA curves of fipronil in isothermal mode at a) 150 °C, b) 160 °C, c) 165 °C, d) 170 °C, e) 175 °C, f) 180 °C, g) 185 °C, h) 190 °C, i) 195 °C, j) 200 °C, k) 205 °C, l) 210 °C, m) 215 °C, and n) 220 °C.

Once the applied isothermal temperature was reached, the sample mass decreased linearly with time for all the samples. However, for the samples heated to higher temperatures, deviations from the expected linear behaviour are evident at longer times. This is attributable to progressive decomposition of fipronil during its exposure to elevated temperatures. It is imperative to minimise potential measurement errors that might result from the effect of such decomposition reactions. In order to avoid this, and also for measurement consistency reasons, all the vapour pressure estimates were based on the mass loss rates measured in the time interval 27.5 to 30 min. The regression parameters obtained for the percentage mass loss versus time for isotherms presented in Fig. 4.5, is given in Table 4.1. The mass of fipronil decreased linearly ($R^2 > 0.9988$), implying that the mass loss followed apparent zero-order kinetics (Table 4.1).

Table 4.1. Regression parameters obtained from the percentage mass loss (y) versus time (x) curves at each temperature.

Temperature (°C)	Linear Regression Equation	Determination Coefficient (R^2)	
150	$y = -0.0322x + 99.916$	0.9990	Sublimation
160	$y = -0.0747x + 100.19$	0.9999	
165	$y = -0.1212x + 100.55$	0.9999	
170	$y = -0.1770x + 101.33$	0.9996	
175	$y = -0.2409x + 100.98$	0.9989	
180	$y = -0.3489x + 103.44$	0.9996	
185	$y = -0.5236x + 107.16$	0.9999	
190	$y = -0.7108x + 110.58$	0.9999	
195	$y = -1.1700x + 116.06$	0.9999	Evaporation
200	$y = -1.6373x + 128.40$	0.9991	
205	$y = -2.2449x + 140.19$	0.9999	
210	$y = -2.8896x + 151.17$	0.9999	
215	$y = -3.6475x + 168.06$	0.9998	
220	$y = -4.3722x + 182.73$	0.9988	

The gradient in these linear regression equations gave the rates of mass loss (*dm/dt*) that were used to determine the nitrogen permeability of fipronil (S_{AB}) and consequently, the vapour pressure.

4.6.2 Vapour pressure predictions for fipronil

The data analysis was based on the assumptions that the vapour behaves as an ideal gas and that the temperature dependence of the vapour pressure follows the integrated Clausius-Clapeyron equation (assuming ΔH is constant) in the temperature range investigated, given in Equation (4).

Linear regression fits of Equation (4) to the experimental S_{AB} data yielded estimates for the parameter values *a*, and *b*. From these, the enthalpies of sublimation, or evaporation, were calculated via the expression $\Delta H_i = bR$.

Fig. 4.6 plots the vapour pressure data for fipronil as extracted from the isothermal TGA curves. The sublimation enthalpy was determined to be 120 ± 4 kJ mol^{-1} while the enthalpy of evaporation was 72 ± 5 kJ mol^{-1}. Based on Hess's Law, the difference between the enthalpies of sublimation and evaporation is the heat of fusion, which amounts to 47.5 kJ mol^{-1}. This is in reasonable agreement with the value, 44.5 kJ mol^{-1}, experimentally obtained by DSC analysis (Fig. 4.1b).

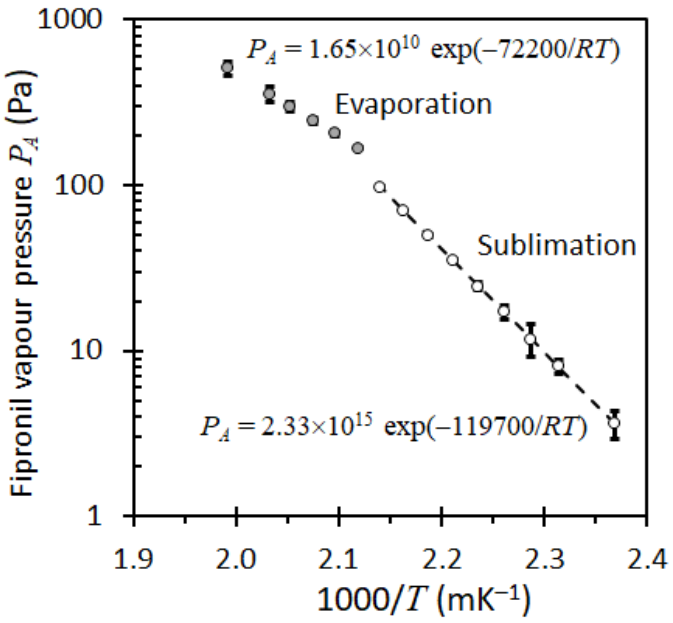

Figure 4.6. Fipronil vapour pressures vs. temperature predicted on the basis of TGA mass loss data.

An alternative method for the determination of vapour pressure using the Eyring equation is presented in Appendix A. Based on this method, the sublimation and the vaporization enthalpies were determined to be 122 kJ mol^{-1} and 91 kJ mol^{-1}. The heat of fusion, calculated by the difference between the enthalpies of sublimation and evaporation was found to be 31 kJ mol^{-1}. This result was not in agreement with the value obtained by DSC analysis. The

two methods predicted the same sublimation enthalpy (±120 kJ mol^{-1}) but the values obtained for the vaporization enthalpies differed substantially.

4.8 Conclusion

TGA experiments were performed with both dynamic and isothermal methods to investigate the thermal characteristics of fipronil. The dynamic TGA results showed that the insecticide displayed a distinct endothermic peak at 201.2 °C upon melting, and exhibited a strong inclination to sublime before this temperature. At higher temperatures, fipronil underwent volatilization, leading to the creation of a non-volatile char residue via a decomposition reaction. The isothermal TGA method was particularly suitable for investigating the vapour pressure of fipronil at higher temperatures. The enthalpies of sublimation and evaporation were calculated, and the collected data suggests that fipronil is likely to sublime when subjected to polymer processing temperatures exceeding 150 °C.

Chapter 5

X-ray diffraction characterization of fipronil polymorphs

5.1 Introduction

The objective of this section of the research was to address the lack of agreement in existing literature regarding the crystal structure of fipronil polymorphs by utilizing powder X-ray diffraction (PXRD) and single crystal X-ray diffraction (SCXRD) to investigate its polymorphic behaviour. Five different crystal forms were obtained by recrystallization from different solvents. These were named PM 1-5, with the prefixed descriptor PM being an abbreviation for PolyMorph. The findings of this investigation are presented in this chapter. Heat treatment at 110 and 150 °C was done on the samples to remove co-crystallized solvents.

5.2 Powder X-ray Diffraction (PXRD)

Powder X-ray diffraction was employed to identify the polymorphic forms present in the bulk samples crystallised from different solvents at room temperature and to identify the role of the solvent in determining which polymorph is obtained. In addition, PXRD confirmed the associations, made on the basis of DSC results (Chapter 6), between the various preparations and specific polymorphs mentioned in the literature.

Fig. 5.1 compares the PXRD patterns obtained from methanol- and acetonitrile-derived fipronil following heat treatment of both samples at 150 °C. The PXRD of the samples obtained by recrystallization from acetone, ethyl acetate and methanol were very similar therefore only one representative pattern is shown. The heat treatment was done in order to remove any co-crystallized solvent or water from the crystal structure.

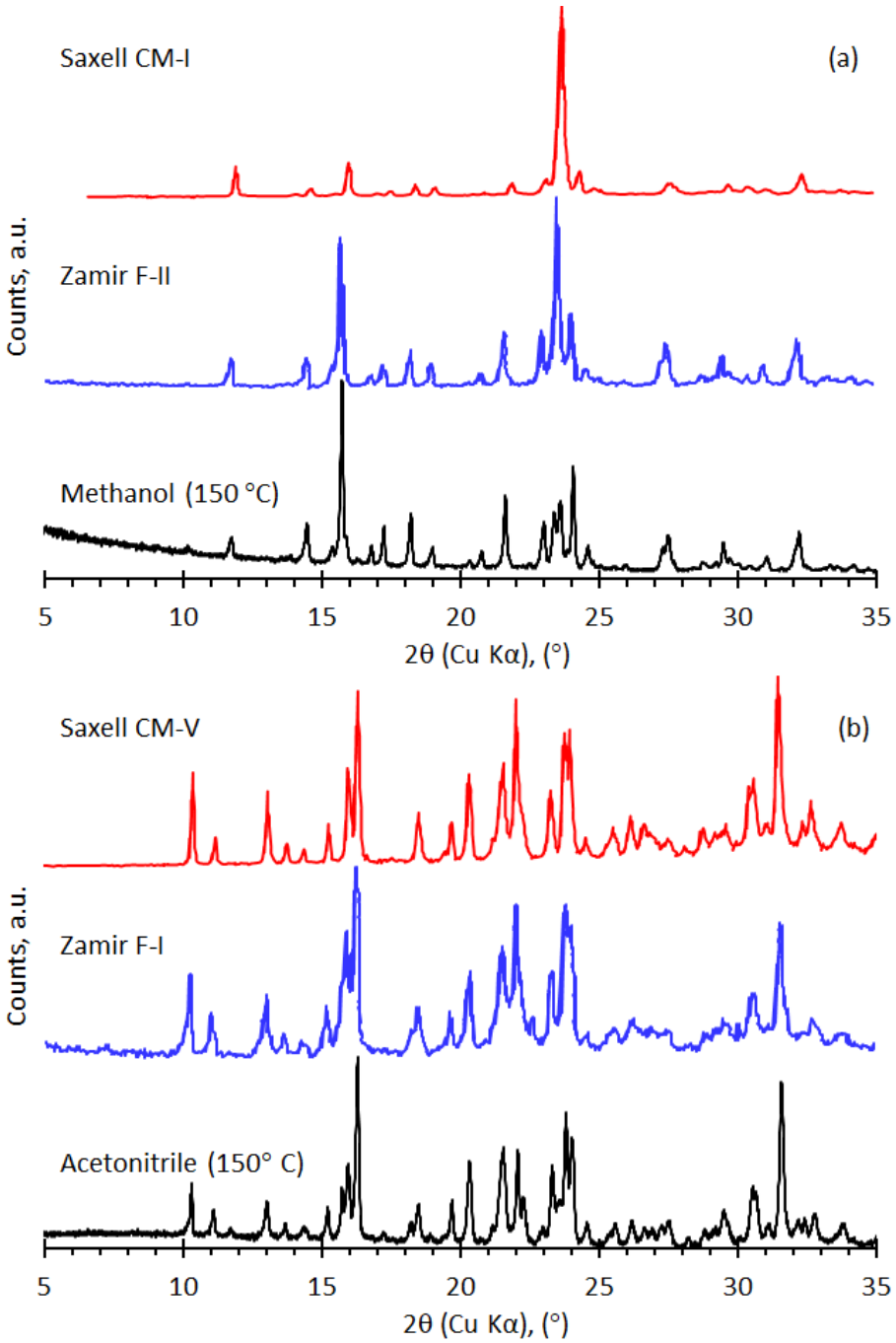

Figure 5.1. Powder X-ray diffractograms for heat treated fipronil samples obtained by recrystallization from (a) methanol and (b) acetonitrile. For comparison, the patterns of solvent-free fipronil polymorphs reported by Saxell et al. (Saxell et al., 2013, Saxell et al., 2018) and Zamir (Zamir, 2015, Zamir, 2013) are also shown.

The diffractogram obtained for the methanol-derived fipronil heat treated at 150 °C (Fig. 5.1a), compares very well with the patterns published by Saxell et al. for CM-I (Saxell et al., 2013) and Zamir for F-II (Zamir, 2015). The diffractograms recorded for all the other samples of fipronil before and after heat-treatment were also very similar as they appeared to be dominated by the reflections typical for CM-I (Saxell et al., 2013) or FII (Zamir, 2015). This implied that all the samples contained very high proportions of this polymorph.

The PXRD pattern for the sample obtained by heat treatment of the acetonitrile-derived sample at 150 °C for 30 min corresponded to that of CM-V and F-I reported by Saxell et al. (2018) and Zamir (2015) respectively.

The PXRD results showed that solvents of crystallization and thermal treatment at 150 °C influenced the polymorphs obtained. Furthermore, heat treatment of the samples confirmed the presence of specific polymorphs, identified in previous literature, for methanol and acetonitrile-derived samples. The results of single crystal X-ray diffraction analysis of the polymorphs are presented in the following section.

5.3 Single Crystal X-ray Diffraction (SCXRD) structure analysis

The powder XRD patterns do not reflect the characteristics of the individual pure phases as some of the samples were, to some extent, mixtures of the various polymorphs. However, it was possible to pick out single crystals from some of the recrystallized fipronil samples and subject them to SCXRD analysis. Five different crystalline forms (polymorphs or pseudo-polymorphs) of fipronil were identified using SCXRD data. These were labelled PM-1 to PM-5. The crystals of forms PM-1 and PM-2 were obtained from acetonitrile, PM-3 was obtained from acetone, PM-4 was crystallized from ethyl acetate, while crystals of PM-5 were grown from methanol. PM-5 was found to correspond to the polymorph reported previously in the literature by Park et al. (2017). Table 5.1 lists the crystallographic parameters of the different

structures. Fig. 5.2 illustrates the asymmetric units of PM-1 to PM-5, with packing diagrams shown in Fig. 5.3. The hydrogen bonding networks present in PM1-PM5 are illustrated in Fig. 5.4.

Table 5.1. Crystallographic data of fipronil polymorphs, solvates and hydrates.

Polymorph	PM-1	PM-2	PM-3	PM-4	PM-5
Crystal system	Monoclinic	Monoclinic	Triclinic	Monoclinic	Monoclinic
Space group	$P2_1/c$	$P2_1/c$	$P\bar{1}$	$P2_1/c$	$I2/a$
a (Å)	8.5926(2)	14.5034(3)	8.65640(10)	14.7036(4)	17.3452(2)
b (Å)	27.0164(14)	31.1201(6)	13.1917(4)	15.5016(6)	12.6351(2)
c (Å)	16.0685(5)	8.71330(10)	16.7395(4)	8.6691(2)	14.9462(2)
α (°)	90	90	99.535(2)	90	90
β (°)	101.026(3)	93.658(2)	103.068(2)	93.796(2)	91.7830(10)
γ (°)	90	90	99.579(2)	90	90
Volume/ Å^3	3661.3(2)	3924.71(12)	1794.47(8)	1971.61(10)	3274.00(8)
Z	4	4	2	4	8
Calculated density (g·cm^{-3})	1.641	1.480	1.633	1.489	1.774
Goodness-of-fit on F^2	1.087	1.098	1.117	1.040	1.041
Final R_1 index [all data]	0.1245	0.0938	0.0921	0.1015	0.0470
wR_2 index [all data]	0.2712	0.2796	0.2472	0.2580	0.1211
$\Delta\rho$ max/min (eÅ^{-3})	1.16/–0.76	1.87/–0.50	1.27/–0.68	0.65/–0.41	0.70/–0.58
Similar structure in literature:	CM-II (Saxell et al., 2011)	-	CM-IV (Saxell et al., 2014)		Park (Park et al., 2017), Saxell (Saxell et al., 2013) CM-I & Zamir F-II (Zamir, 2015)

a, *b*, *c* are the lengths of the unit cell edges; α, β, γ are the angles of the unit cell, *Z* represents the number of molecules in the unit cell and ρ is the calculated density.

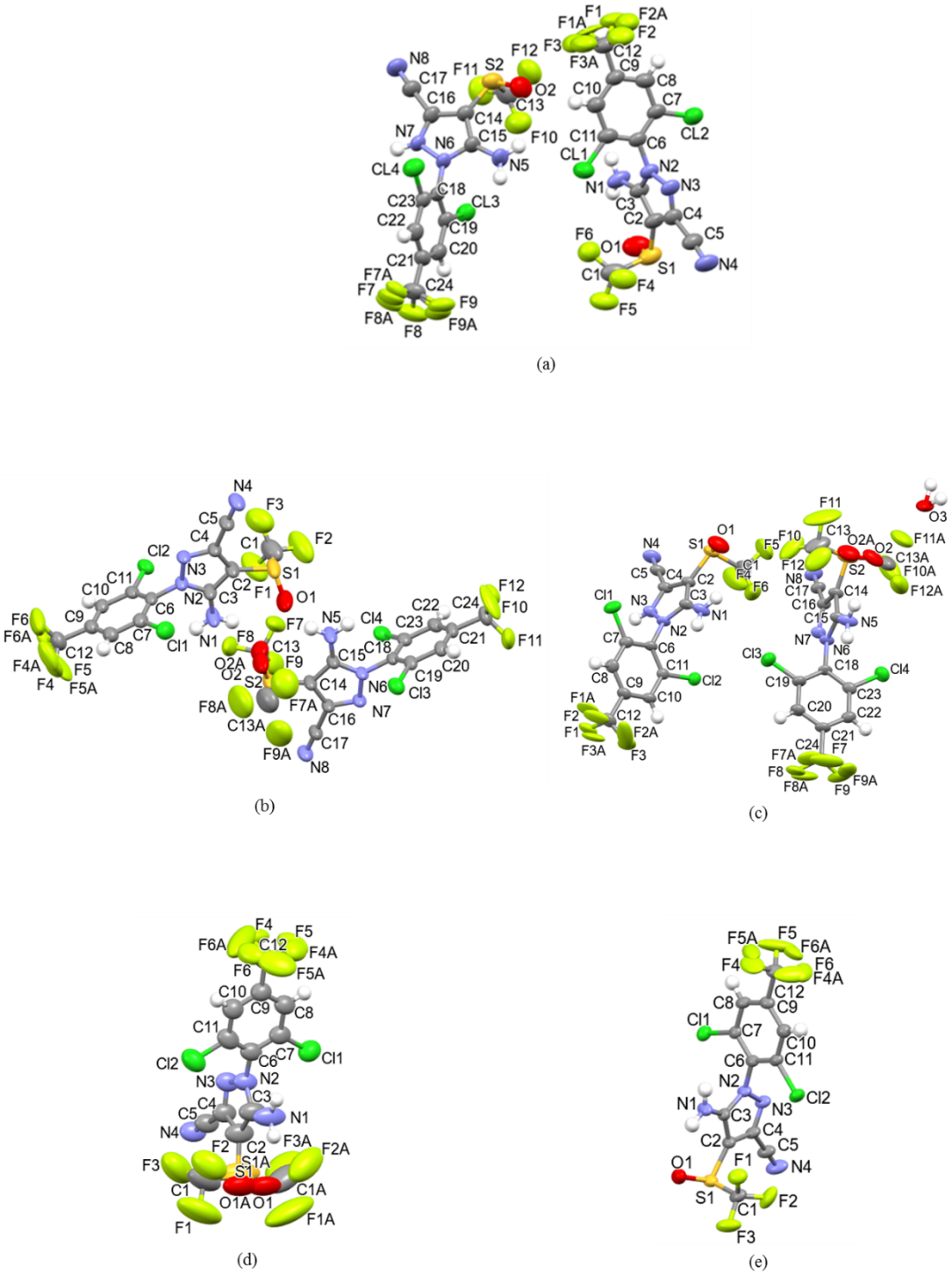

Figure 5.2. Asymmetric units of (a) PM-1 (b) PM-2 (c) PM-3 (d) PM-4 and (e) PM-5. Ellipsoids are drawn at the 50% probability level, and hydrogen atoms are illustrated as white spheres of arbitrary size.

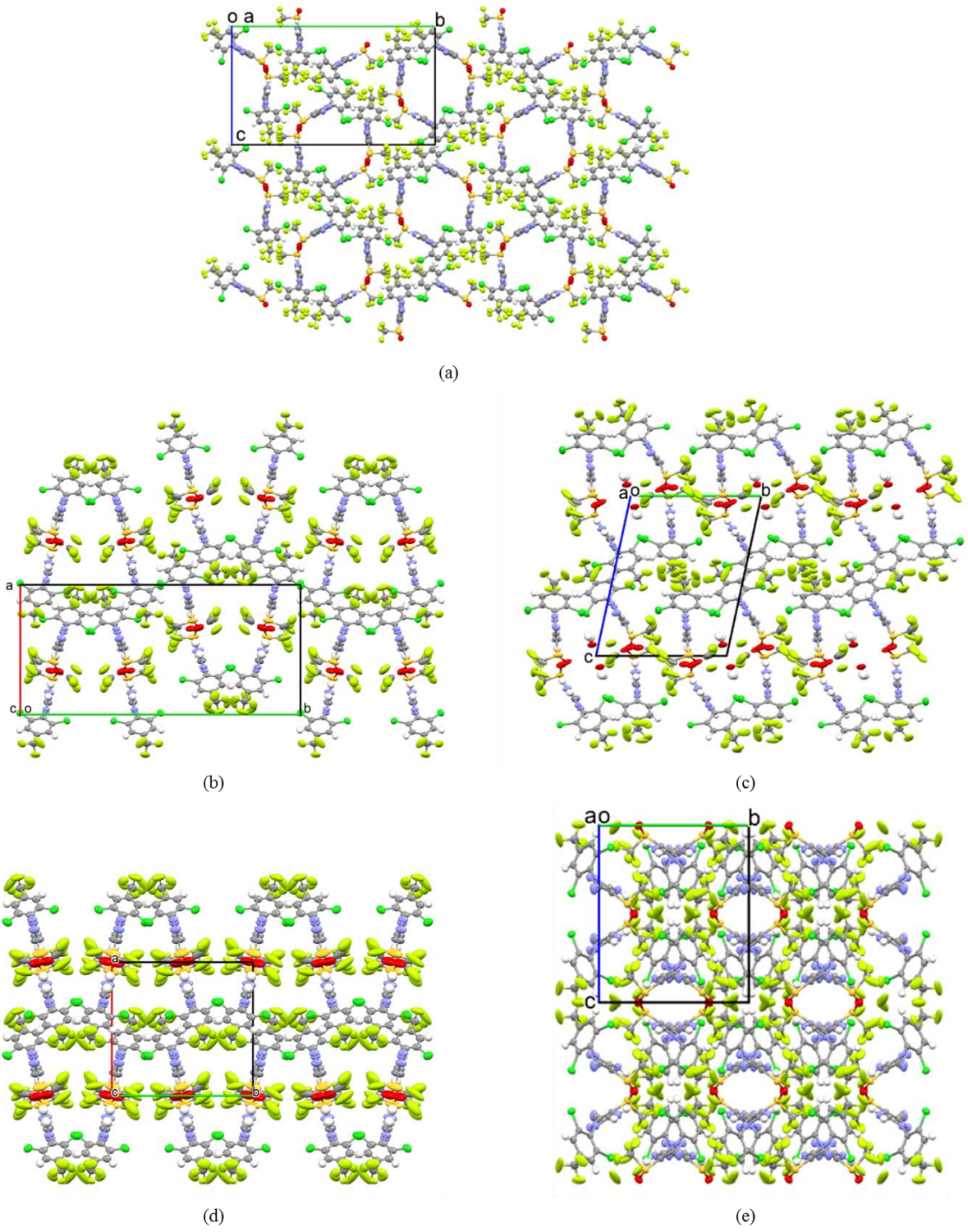

Figure 5.3. Packing diagrams of (a) PM-1 viewed down the *a*-axis (b) PM-2 viewed down the *c*-axis (c) PM-3 viewed down the *a*-axis (d) PM-4 viewed down the *c*-axis and (e) PM-5 viewed down the *a*-axis.

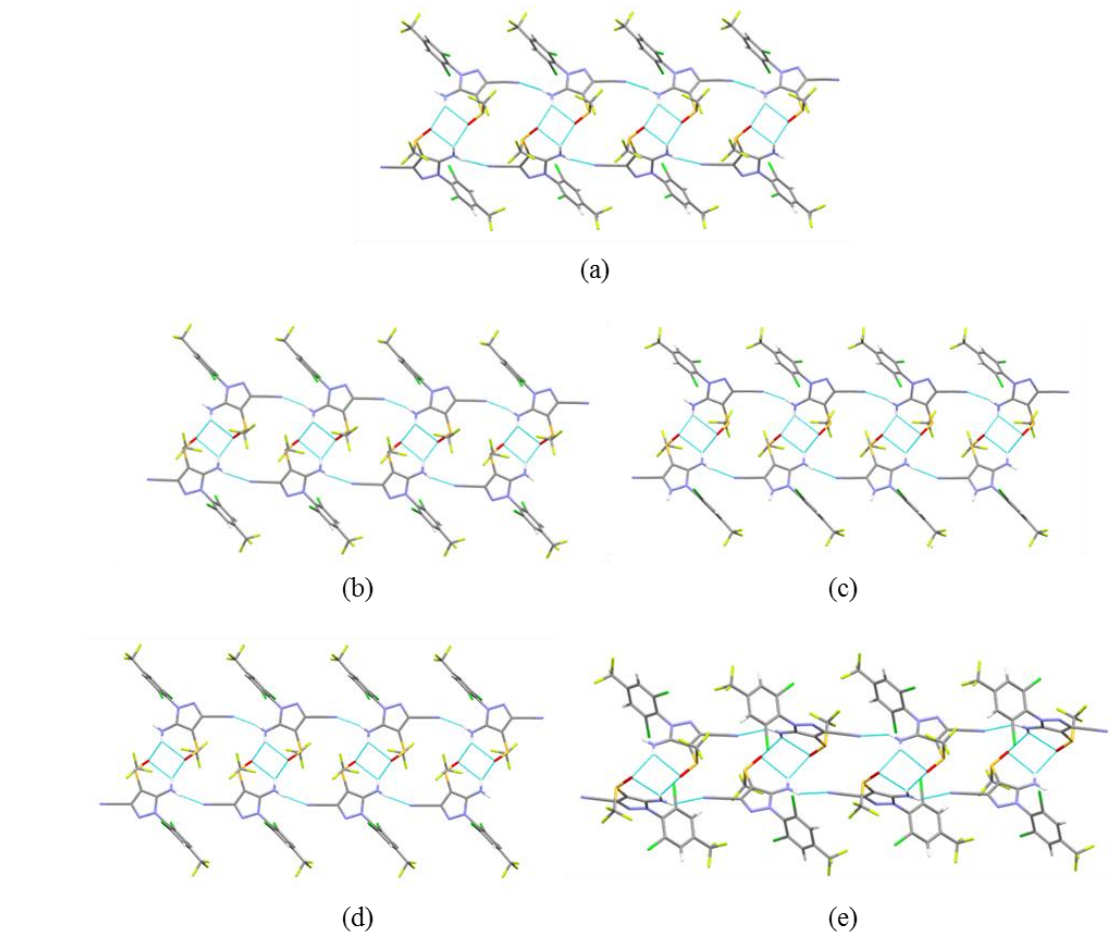

Figure 5.4. Hydrogen bonding interactions in (a) PM-1 (b) PM-2 (c) PM-3 (d) PM-4, and (e) PM-5.

5.3.1 Form PM-1

PM-1 was obtained by crystallization from acetonitrile at room temperature. This form was similar to Saxell's crystalline modification CM-II. The pseudo-polymorph crystallizes in the space group $P2_1/c$, with the asymmetric unit comprised of two crystallographically independent fipronil molecules, as shown in Fig. 5.2a, with the molecule containing atom S1 labelled molecule A, and the molecule containing atom S2 denoted molecule B. In both molecules A and B, the trifluoromethyl group attached to the benzene ring is disordered over two positions, with relative occupancies of 0.781(11) and 0.219(11) in molecule A and 0.56(2) and 0.44(2) in molecule B. In molecule A, the planes through the benzene and pyrazole groups form an angle

of 81.25°, with the corresponding angle having a value of 78.55° in molecule B. These relative ring orientations, leaning towards 90°, are primarily due to steric effects where the 2,6-dichloro substituents on the aryl ring would come into close contact or even overlap in space with the NH_2 substituent and N3-atom of the pyrazole ring in the case of the two planes bisecting at 0°. In general, the bonding distances of the respective functional groups all fall within the expected ranges (Park et al., 2017).

Fig. 5.3a illustrates the packing of the molecules as viewed down the *a*-axis. It is evident, from the packing diagram, that channels are present in the structure. These are assumed to be occupied by acetonitrile solvent molecules, making PM-1 a pseudo-polymorph of fipronil. However, the acetonitrile solvent molecules could not be located reliably in the electron difference map, hence the SQUEEZE command was employed in the refinement of the structure where the diffuse contribution to the overall scattering of one molecule of acetonitrile was considered.

In both molecules A and B, each NH_2 group (N1) forms two hydrogen bonds. Firstly, a bifurcated hydrogen bond is formed to two oxygen atoms (O1, O2) of two different sulfinyl groups, with one hydrogen bond intramolecular (N1-H1B···O1), and one intermolecular (N1-H1B···O2). The second hydrogen atom on the amine group (N1-H1A) forms an intermolecular hydrogen bond to the nitrogen atom (N4) of a nitrile group on a different molecule. Fig. 5.4a illustrates the resulting hydrogen bonded ribbon. Molecule's A form propagates on the one side of the hydrogen bonded ribbon, and molecule's B form the opposite side of the ribbon. Distinct hydrogen bonding networks may also be described in terms of graph sets: two unique parallel chains (the one involving molecule A and the other molecule B) may each be defined as *C*(7), whereas the intramolecular hydrogen bond between the amine and sulfinyl group may be defined as *S*(6). Two unique rings are also observed, the one involving two molecules, $R_2^2(4)$, and a larger ring incorporating four different molecules, $R_4^4(18)$. It is interesting to note that all

five structures PM-1 to PM-5 exhibited identical hydrogen bonding patterns and graph sets (*vide infra*), despite their unique structures and packing in three dimensions. Additionally, one of the hydrogen atoms on the amine group of molecule B forms a hydrogen bond to a chlorine atom on a neighbouring molecule, effectively making this a trifurcated hydrogen bond. This interaction is not observed for molecule A. Hydrogen bonding parameters are listed in Table 5.2.

Table 5.2. Selected hydrogen bonding parameters (Platon) for Polymorphs PM-1 to PM-5.

Form	D-H···A	D-H (Å)	H···A (Å)	D···A (Å)	D-H···A (°)	Symmetry
PM-1	N1-H1A···N4	0.8800	2.2000	3.0647	168.00	–1+x,y,z
	N1-H1B···O1	0.8800	2.4100	3.0146	126.00	-
	N1-H1B···O2	0.8800	2.2400	2.9996	144.00	x,1/2-y,-1/2+z
	N5-H5A···N8	0.8800	2.1800	3.0483	168.00	1+x,y,z
	N5-H5B···O2	0.8800	2.4100	2.9935	124.00	-
	N5-H5B···O1	0.8800	2.2300	2.9609	140.00	x,1/2-y,1/2+z
PM-2	N1-H1A···N4	0.8800	2.2000	3.0571	166.00	x,y,1+z
	N1-H1B···O2	0.8800	2.1600	2.8862	140.00	-
	N5-H5A···N8	0.8800	2.1700	3.0219	163.00	x,y,-1+z
	N5-H5B···O2	0.8800	2.1100	2.8811	146.00	-
	N5-H5B···O1	0.8800	2.5500	3.1136	123.00	-
PM-3	N1-H1A···N4	0.8800	2.2100	3.0815	169.00	1+x,y,z
	N1-H1B···O2	0.8800	2.3000	2.9184	127.00	x,y,1+z
	N1-H1B···O2A	0.8800	2.1800	2.9813	152.00	–1+x,y,z
	N5-H5A···N8	0.8800	2.1700	3.0309	167.00	x,y,-1+z
	N5-H5B···O1	0.8800	2.0800	2.8508	146.00	-
	N5-H5B···O2A	0.8800	2.5000	3.0861	125.00	-
PM-4	N1-H1A···N4	0.8800	2.1700	3.0305	166.00	x,y,1+z
	N1-H1B···O1	0.8800	2.5400	3.1059	123.00	-
	N1-H1B···O1	0.8800	2.1300	2.8838	144.00	–x,1-y,1–z
	N1-H1B···O1A	0.8800	2.1000	2.8784	146.00	–x,1-y,1–z
PM-5	N1-H1A···N4	0.8800	2.3800	3.1728	151.00	–1/2+x,1–y,z
	N1-H1B···O1	0.8800	2.5100	3.0909	124.00	-
	N1-H1B···O1	0.8800	2.2800	2.8945	127.00	1/2-x,y,–z

5.3.2 Form PM-2

PM-2 was crystallized from acetonitrile at room temperature and was found to be a concomitant polymorph to PM-1, since it formed in the same crystallization vessel as pseudo-polymorph PM-1. PM-2 crystallizes in the space group $P2_1/c$, and does not contain any solvent molecules, hence it is a polymorph of fipronil.

The asymmetric unit of PM-2 comprises two fipronil molecules, which will be denoted molecule A, containing nitrogen atom S1, and molecule B, containing nitrogen atom S2. Both molecule A and molecule B contain disordered trifluoromethyl groups, however, the two molecules differ in the type of disorder exhibited by the groups. In molecule A the fluorine atoms of the trifluoromethyl group bonded to the benzene group are disordered over two positions, with an occupancy of 0.566(10) and 0.434(1). The entire trifluoromethyl group bonded to the sulphur atom is disordered over two positions in molecule B, with the two disordered portions on opposite sides of the sulphur atom, with occupancies of 0.6 and 0.4, respectively.

The angle between the plane through the benzene group and the plane through the pyrazole group is 81.26° in molecule A and 81.59° in molecule B, which are comparable with those in PM-1.

The packing diagram of PM2 is illustrated in Fig. 5.3b A sinusoidal, layered packing is exhibited, with benzene groups and their attached substituents packing in a layer, the tetrafluoromethanesulfinyl groups packing in a layer, and the pyrazole groups packing in two different layers.

As illustrated in Fig. 5.4b, one of the hydrogen atoms of an amine group of molecule A (or molecule B) forms a bifurcated hydrogen bond between its own sulfinyl group, and the sulfinyl group of a molecule B (or molecule A), thus the bifurcated hydrogen bond is both

intramolecular and intermolecular. At the same time, the second hydrogen atom on the amine group of molecule A (or molecule B) forms a hydrogen bond to the nitrile group of a different molecule A (or molecule B). These interactions result in a hydrogen bonded ribbon consisting of hydrogen bonded molecules A and B, as illustrated in Fig. 5.4b.

5.3.3 Form PM-3

PM-3 crystallizes in the space group $P\bar{1}$, and was obtained from acetone. Its structure was found to contain solvent water molecules, which were presumed to have been present in the acetone solvent used for crystallization, making it a pseudo-polymorph of fipronil. PM-3 is a hemihydrate of fipronil. A similar form was obtained by Saxell and co-authors (Saxell et al., 2014) and named crystalline modification CM-IV.

The asymmetric unit of PM-3 contains two fipronil molecules and one water molecule, with the fipronil molecules showing disorder in their trifluoromethyl groups (Fig. 5.2c). The molecule containing atom S1 will be denoted molecule A, and the one containing atom S2 molecule B. In both molecules the fluorine atoms of the trifluoromethyl group on the benzene ring are disordered over two positions, with an occupancy of 0.773(15) and 0.227(15) in molecule A, and 0.457(19) and 0.543(19) in molecule B. In molecule B, the trifluoromethyl group attached to the sulphur atom is disordered over two positions, on opposite sides of the sulphur atom, with an equal occupancy of 0.5 each. The plane through the benzene group and the plane through the pyrazole group form an angle of 80.65° in molecule A and 84.03° in molecule B.

As can be seen from Fig. 5.3c, a layered structure is formed, with the benzene groups and their attached substituents packing in a layer, the tetrafluoromethanesulfinyl groups packing in a layer, and the pyrazole groups packing in two different layers. The water molecules pack in rows along the *a*-direction.

Exactly the same hydrogen bonding interactions that were found to be present between the fipronil molecules in PM-2, are present in PM-3. These result in a hydrogen bonded ribbon, as depicted in Fig. 5.4c. Additionally, the water molecules are involved in hydrogen bonding, with each water molecule forming two hydrogen bonds to two different chlorine atoms on two different neighbouring fipronil molecules.

5.3.4 Form PM-4

PM-4 crystallized from acetonitrile at room temperature in the space group $P2_1/c$, with one fipronil molecule in the asymmetric unit. In this molecule, the trifluoromethylsulfinyl group and the fluorine atoms on the trifluoromethyl group on the benzene ring are disordered over two positions, with the first showing an equal occupancy of 0.5, and the second an occupancy of 0.622(8) and 0.378(8). As can be seen in Fig. 5.2d, the disordered trifluoromethulsulfinyl groups are positioned on opposite sides of the pyrazole plane, with the pyrazole plane forming an angle of 86.78° with the benzene plane.

The packing of fipronil molecules in this polymorph, as viewed down the *c*-axis, is illustrated in Fig. 5.3d. A layered structure is formed, with the benzyl groups packing in a layer, and the trifluoromethulsulfinyl packing in another layer. The packing of molecules is similar to the packing observed in PM-2, however the layers are more wavy in PM-2.

Identical hydrogen bonding interactions between fipronil molecules in PM-2 and PM-3 are present (Fig. 5.4d).

5.3.5 Form PM-5

PM-5 was crystallized from methanol at room temperature and corresponds to the structure of fipronil reported in the literature, with CSD (Version 5.43, September 2022 update) reference code YEGJAY (Park et al., 2017). The literature structure was reported in setting *C*2/*c* of space group 15, however, in the current study it has been determined in the conventional setting *I*2/*a*.

Since a detailed discussion of this structure has been published (Park et al., 2017), only the major structural features will be highlighted here, especially with reference to the other polymorphs or pseudo-polymorphs.

The asymmetric unit of PM-5 is comprised of one fipronil molecule, with the trifluoromethyl group on the benzene ring disordered over two positions, with occupancies of 0.611(16) and 0.389(16). Interestingly, the same disorder is present in the structure in YEGJAY, where they found occupancies of 0.620(15) and 0.380(15). In the structure of PM-5, the plane through the benzene group and the plane through the pyrazole group form an angle of 89.69°, closely corresponding to the same angle in YEGJAY (89.03(9)°). This angle is the closest to 90° of all the plane dihedral angles in forms PM-1 to PM-5, with molecule A of PM-3 having the smallest angle of 80.65°.

The packing diagram of fipronil molecules in PM-5, viewed down the *a*-axis, is shown in Fig. 5.3e. Channels extending along the *a*-direction is evident from packing along the *a*-axis. It is presumed that these channels were occupied by methanol solvent molecules during crystallization, evaporating over time leaving the crystal lattice intact. The precise location of the solvent molecules could not be placed in the electron density map due to little or no density observed in the voids. The same hydrogen bonding interactions present between fipronil molecules in PM-1 to PM-4 are present in PM-5, as illustrated in Fig. 5.4e.

5.4 Conclusion

PXRD analysis of the bulk samples obtained from different solvents confirmed the presence of several polymorphs. SCXRD analysis revealed the existence of five distinct forms of fipronil named polymorphs 1-5 (PM1-PM-5). The results are summarised in Table 5.3.

Table 5.3. Summary of solvent systems used to obtain polymorphs 1-5.

Solvent	Polymorphs obtained
Acetonitrile (room temperature)	PM-1, PM-2, PM-5
Ethyl acetate (room temperature)	PM-1, PM-4, PM-5
Ethyl acetate (low temperature)	PM-4
Acetone (room temperature)	PM-3
Methanol (room temperature)	PM-5

When crystallized from acetonitrile or ethyl acetate at room temperature, concomitant polymorphism was observed. Forms PM-1, PM-2, and PM-5 were obtained from the former solvent, while forms PM-1, PM-4, and PM-5 were obtained from the latter. Crystallization from acetone at room temperature exclusively yielded PM-3, while PM-5 was exclusively obtained from crystallization from methanol at room temperature. Pure PM-4 was obtained by cooling acetonitrile in a refrigerator and then crystallizing from it.

Recrystallization of fipronil from acetonitrile resulted in a mixture of different polymorphs or pseudo-polymorphs. However, subjecting the product to heat treatment for 30 minutes at 150°C yielded a nearly pure polymorph that exhibited PXRD and thermal properties consistent with crystal modification CM-V described by Saxell et al. (2018) and form F-I reported by Zamir (2015). On the other hand, recrystallization from methanol did not produce a solvate, but instead yielded a near-pure polymorph referred to as PM-5. Its PXRD pattern was similar to that of crystal modification CM-I reported by Saxell et al. (2018) and form F-II disclosed by Zamir (2015), and closely resembled the pattern predicted based on the single crystal data published by ark et al. (2017). All investigators agreed that this polymorph belongs to the monoclinic crystal system, but there were differences in space group indexing. While the present analysis indexes this polymorph into space group *I*2/*a*, Tang et al. (2005) suggested *P*21/*n* while both Saxell et al. (2013) and Park et al. (2017) indicated space group C2/c instead.

The crystal structures determined for the solvates PM-2, PM-3 and PM-4 showed a degree of similarity in terms of the packing of the molecules. However, the structures PM-1 and PM-5 were significantly different from each other, and from the rest of the structures. Of interest is the fact that, despite the structural differences, the same basic hydrogen bonding motif is present in all the structures.

Thermal analysis was then carried out in order to detect and differentiate between different polymorphic forms present in the bulk samples of recrystallised fipronil. This was done by investigating the qualitative and quantitative data on the thermal behaviour of the different polymorphs and is reported in the next chapter.

Chapter 6

Characterization of the thermal phase behaviour of fipronil polymorphs

6.1 Introduction

The results presented in Chapter 4 showed that fipronil displayed a distinct endothermic peak at 201.2 °C upon melting and exhibited a strong inclination to sublime before it melts. For this reason, the sublimation product and its associated residue were collected through a sublimation setup by which the sublimate was collected after condensation on a cold finger. It was deemed important to determine whether there are any differences between the thermal behaviour of the neat fipronil, the sublimate and the sublimation residue.

PXRD results (Chapter 5.2) showed that recrystallization in specific solvents and temperatures influenced the polymorphs obtained. Furthermore, heat treatment of the samples at 150 °C confirmed the presence of specific polymorphs, identified in previous literature, for methanol and acetonitrile-derived samples. SXRD results (Chapter 5.3) proved the existence of five polymorphs of fipronil, obtained from crystallization of the neat fipronil in various solvent systems. A summary of the solvent systems used to obtain these polymorphs was given in Table 5.3.

This chapter presents the results of the thermal characterization of neat, as-received fipronil, the sublimation product and residue, as well as the bulk samples of fipronil recrystallized from different solvent systems using differential scanning calorimetry (DSC) and thermogravimetric analysis (TGA). In addition, heat treatment at 110 and 150 °C was performed in a laboratory oven on the neat fipronil and the samples recrystallized from the different solvents in order to

investigate the effect thereof on loss of solvent and thermal behaviour of the polymorphs identified by single crystal X-ray diffraction analysis (SCXRD).

6.2 Thermogravimetric analysis (TGA) of neat fipronil, sublimate, and recrystallized samples

Thermogravimetric analysis of neat, as-received fipronil at different heating rates from 1 to 10 °C was carried out in order to investigate the effect of heating rate on the thermal behaviour of the neat fipronil sample. The results of the analyses are given in Fig. 6.1.

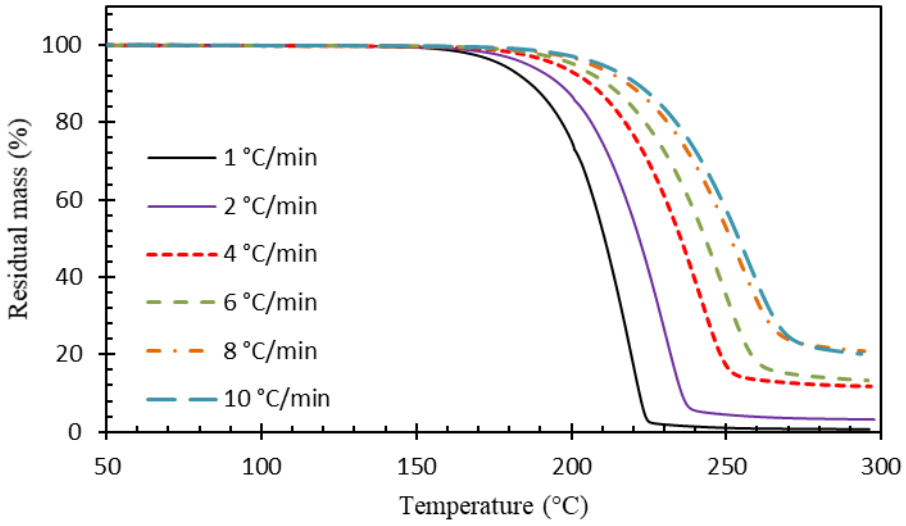

Figure 6.1. Thermogravimetric analysis (TGA) curves for neat fipronil at different heating rates.

The results obtained showed that at the lowest heating rate (1 °C min^{-1}) mass loss started above ca. 140 °C and occurred in a single step resulting in complete mass loss by 280 °C. This mass loss was ascribed (Chapter 4.2) to sublimation of the solid and complete evaporation of the molten fipronil over the temperature range studied.

As thermo-analytical techniques are deeply influenced by experimental conditions (Brown, 2001), as expected, increasing the heating rate shifted the TGA curves to a higher temperature

region and resulted in the formation of thermally stable char residues, evident by incomplete mass loss observed in the TGA curves. The char yields varied from about 3% by mass using a heating rate of 2 °C min^{-1} to as much as 20% by mass at a heating rate of 10 °C min^{-1} (Fig. 6.1a). The formation of the thermally stable solid residues suggested some degree of thermal decomposition at the higher heating rates. The selection of a heating rate of 2 °C min^{-1} for further TGA analyses was based on two factors: minimizing the degree of decomposition of fipronil and allowing for efficient analysis of multiple samples within a reasonable timeframe.

TGA analysis was performed on the sublimation product, obtained under vacuum at temperatures between 150 and 190 °C. The results are shown in Fig. 6.2.

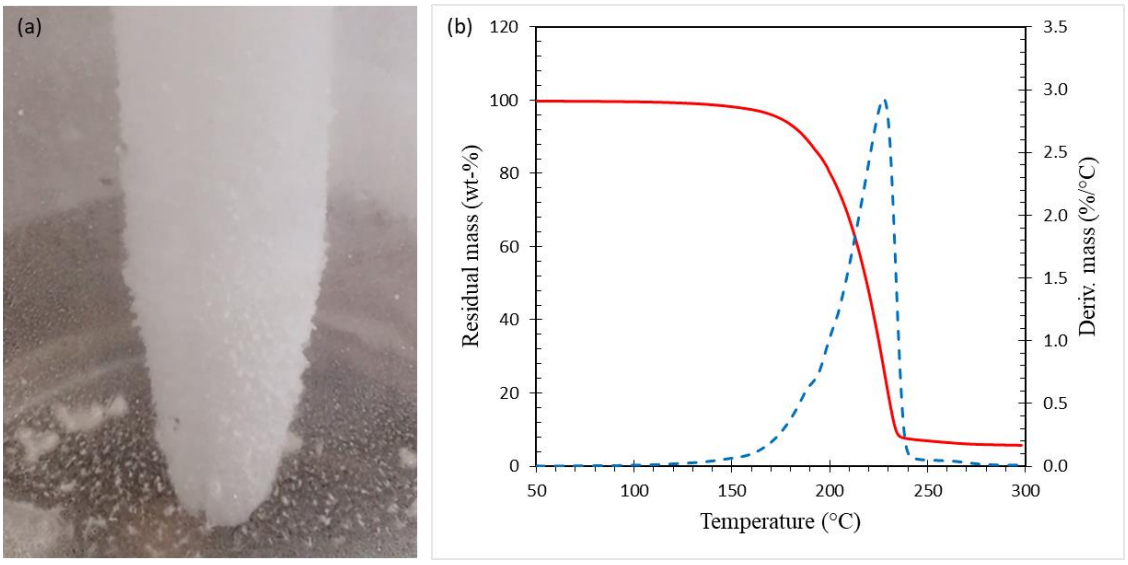

Figure 6.2. (a) White, fluffy sublimation product on the cold finger of the sublimation apparatus, (b) TGA and DTG curves of the sublimated product. B = 2 °C min^{-1}.

The sublimate was a white, fluffy powder that collected on the cold finger of the sublimation apparatus (Fig. 6.2a). Thermogravimetric analysis of the product (Fig. 6b) showed that mass loss of the sublimated form starts at a much lower temperature (~110 °C) than was observed for neat fipronil, as seen in the DTG curve. The rest of the TGA curve followed the same trend

as observed for neat fipronil except for the deviation after melting observed in the DTG curve (Fig. 6.1).

Fig. 6.3 shows the TGA and DTG curves for samples obtained by recrystallization from acetonitrile, acetone, ethyl acetate and methanol.

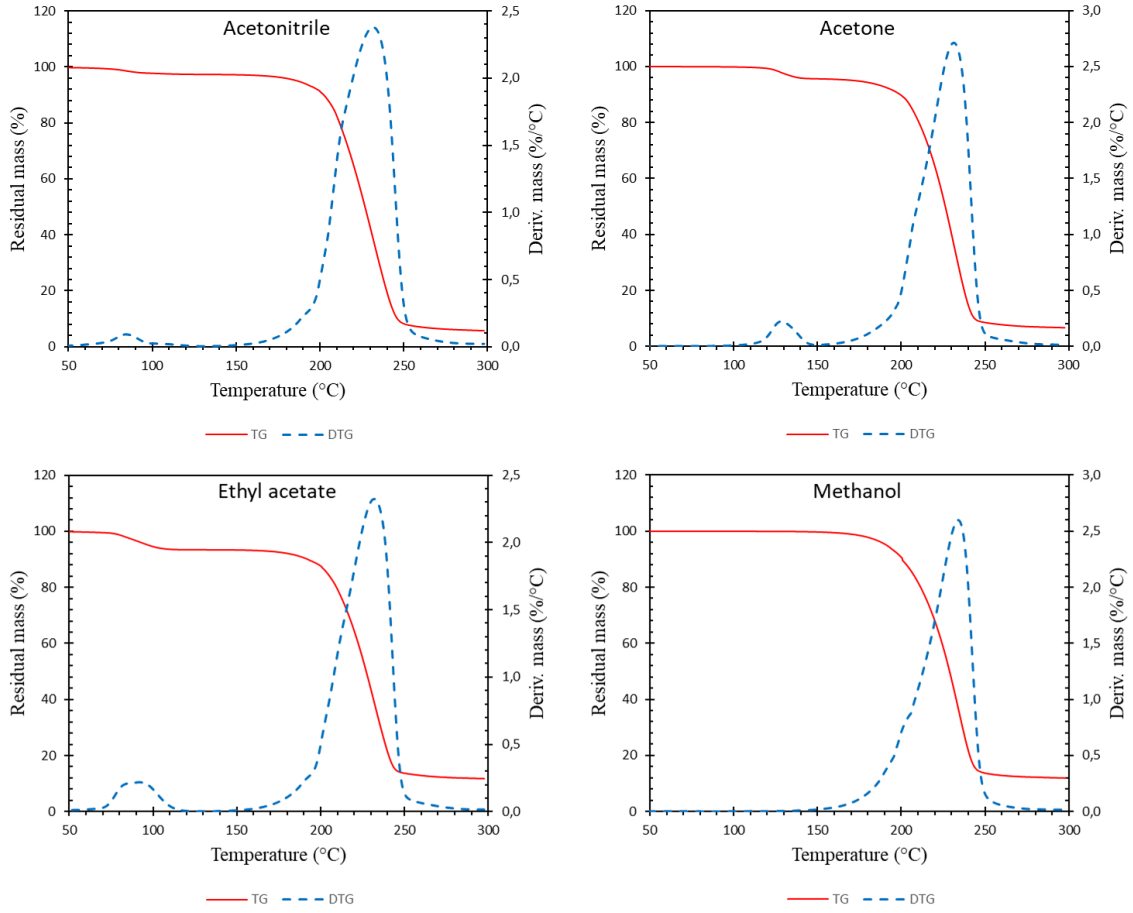

Figure 6.3. Thermogravimetric (TGA) and differential mass change (DTG) curves for fipronil samples recrystallized from acetonitrile, acetone, ethyl acetate and methanol. β = 2 °C min^{-1}.

The TGA and DTG curves for the acetonitrile-derived sample showed an initial mass loss between 60 °C and 100 °C. A similar minor mass loss, ascribed to removal of the solvent, occurred in the acetone-derived sample and in the sample recrystallized from ethyl acetate.

However, for the acetone-derived sample, loss of solvent only occurred between 115 °C and 145 °C. Saxell et al. (2011) also commented on the observation that acetone is only removed at temperatures above 120 °C during TGA analysis. This was unexpected since the boiling point of acetone (56 °C) is lower than the boiling points of the other recrystallizing solvents (Table 6.1). The result confirmed the results obtained for the crystal structure of polymorph 3 (PM-3) whose structure contained solvent water molecules. The other solvents were all lost at much lower temperatures that corresponded to the respective boiling points. The absence of a mass loss event below 150 °C for the methanol-derived sample indicated that a solvate did not form by recrystallization from methanol. The TGA curves obtained for the as-received neat fipronil (Fig 6.1), the fipronil sublimate (Fig 6.2) and the heat-treated fipronil samples (results not shown) were similar to that of the methanol-derived material.

Zamir (2015) suggested that fipronil forms hemi-solvates with some solvents, i.e. that the solvates contain one molecule of the solvent for every two molecules of fipronil. The ratio of the number of fipronil molecules to solvent molecules of the samples recrystallized in this study was estimated from the TGA mass loss values recorded at a temperature of 150 °C. The ratios estimated for triplicate TGA measurements of the acetone derived sample were 2.23, 2.91 and 3.07; for acetonitrile they were 2.00, 3.25 and 3.39 while for ethyl acetate a value of 2.11 was found. The lower measured values were close to two, the value expected for a hemi-solvate. However, some values were somewhat higher, suggesting that if hemi-solvate formation were indeed possible, the available spaces inside the fipronil channels of some of the present samples were not fully occupied by guest solvent molecules.

Slow mass loss, due to sublimation, commenced at temperatures just above 150 °C for all samples after the complete loss of solvent. Rapid mass loss, attributed to evaporation, was seen in the TGA curves of all samples once the temperature exceeded 190 °C. However, a thermally

stable char residue remained after about 250 °C implying thermal decomposition. The char yield varied from about 6% by mass for the acetonitrile- and acetone-derived samples to approximately 12% by mass for the methanol-derived fipronil sample (Fig. 6.1).

6.3 DSC analysis of fipronil polymorphs

6.3.1 DSC analysis of neat fipronil, the sublimate and sublimation residue

DSC analysis was carried out on the bulk samples in order to investigate whether the technique could be used to detect and differentiate between different polymorphic forms, as well as to gain qualitative and quantitative information about the thermal behaviour of the polymorphic forms. Fig. 6.4 shows the DSC curves recorded for the as-received neat fipronil (a) before and after heat treatment at 110 °C and (b) an extract of the peaks in the temperature range 180-220 °C.

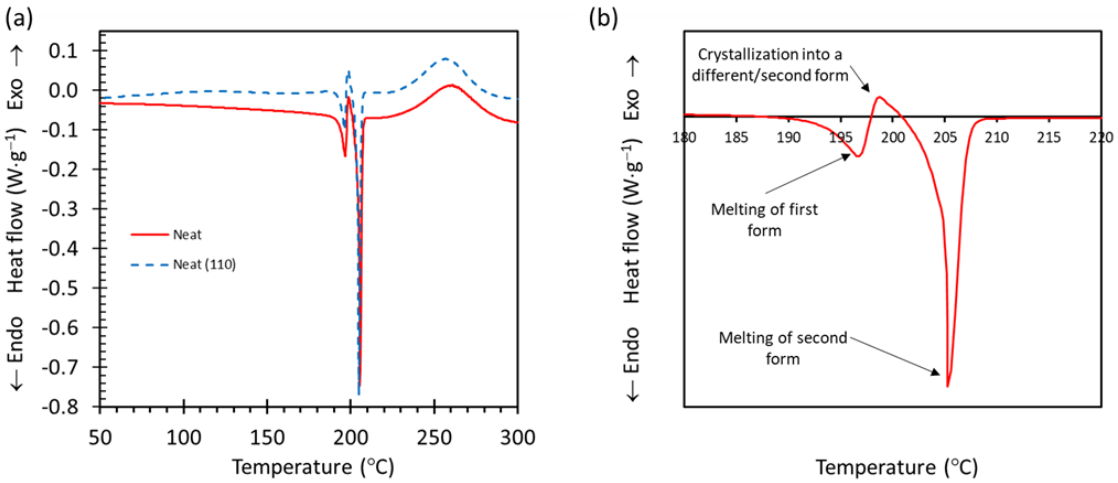

Figure 6.4. DSC curves obtained for neat fipronil (a) before (red) and after (blue) heat treatment and (b) an extract of the peaks showing melt-recrystallization-melt transitions in the temperature range 180-220 °C. β = 5 °C min^{-1}.

The DSC curves of the two fipronil samples (Fig. 6.4a) showed four thermal transitions during heating. The first endothermic peak, attributed to melting, occurred with an onset at 193.2 °C,

peak maximum at 197.0 °C and ΔH_m = 21.2 J g^{-1}. This was followed by a small exothermic event at ~202 °C (ΔH_c = –5.1 J g^{-1}), attributed to recrystallization of the melt. Immediately thereafter, a second endothermic transition with a peak temperature of 206.0 °C (ΔH_m = 87.1 J g^{-1}), due to a second melting process, was observed. The fourth transition was a broad exotherm with an onset at 246 °C and peak maximum at 260 °C due to the decomposition of fipronil. The presence of two melting endotherms, which were also observed on a hot stage microscope, may indicate the presence of a mixture of two polymorphic forms in the neat fipronil sample. This data confirmed that of Zamir (2013), who suggested that pure Form F-II (similar to CM-I reported by Saxell et al. (2018)) exhibited two melting endotherms. However, Saxell et al. (2013) and Saxell et al. (2014) were able to prepare a sample of crystalline modifications CM-I which featured a single melting endotherm with a peak maximum between 196 - 199 °C (Saxell et al., 2013).

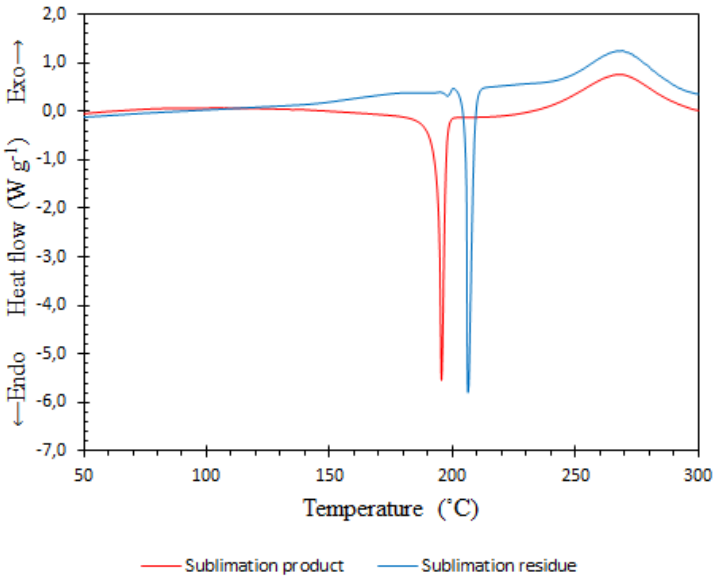

Figure 6.5. DSC curves for the sublimate and the recovered residue from the sublimation experiment. β = 5 °C min^{-1}

Fig. 6.5 shows the DSC curves recorded for the purified sublimate and the residue which remained at the bottom of the flask after incomplete sublimation (Fig. 6.2a). The sublimate sample formed at low temperatures as it was collected on the cold finger of the sublimation apparatus. It featured a lower melting point (195.4 °C) than the sublimation residue (206.1 °C) which was, in effect, heat-treated at about 180 °C during the sublimation experiment. The sublimate and sublimation residue were identified by PXRD as the polymorphs CM-I (PM-5) and CM-V, reported by Saxell et al. (2018), respectively.

Table 6.1 summarises the DSC parameters (temperature and enthalpy values) of the observed transitions for the neat fipronil, the purified sublimate and the residue which remained at the bottom of the flask after incomplete sublimation.

Table 6.1. DSC parameters obtained for neat fipronil, fipronil heat treated at 150 °C, the sublimate and sublimate residue.

Sample	**m.p. onset (°C)**	T_{m1} **(°C)**	T_{m2} **(°C)**	ΔH_{m1} **(J·g^{-1})**	ΔH_{m2} **(J·g^{-1})**
Neat	193.2	197.0	205.8	21.2	87.1
Neat (150)*	193.8	196.3	204.6	17.3	89.9
Sublimate	193.3	195.4	-	96.8	-
Sublimate residue		-	206.1	-	95.3

m.p.: melting point; T_{m1} and ΔH_{m1}: temperature and enthalpy change associated with the first melting endotherm; T_{m2} and ΔH_{m2}: temperature and enthalpy change associated with the second melting endotherm
*: value in brackets indicate temperature of heat treatment in °C

The data in Table 6.1 confirms that the neat, as-received fipronil is a mixture of two polymorphs. Sublimation was used to successfully separate the two polymorphs in the form of a sublimate and sublimate residue with peak melting temperatures at 195.4 and 206.1°C, respectively.

Fig. 6.6 shows the effect of varying the heating rate on the DSC curves of neat fipronil. The heating rate is a decisive parameter which can determine the extent and mechanism of polymorphic transformation (Aronhime, 1988).

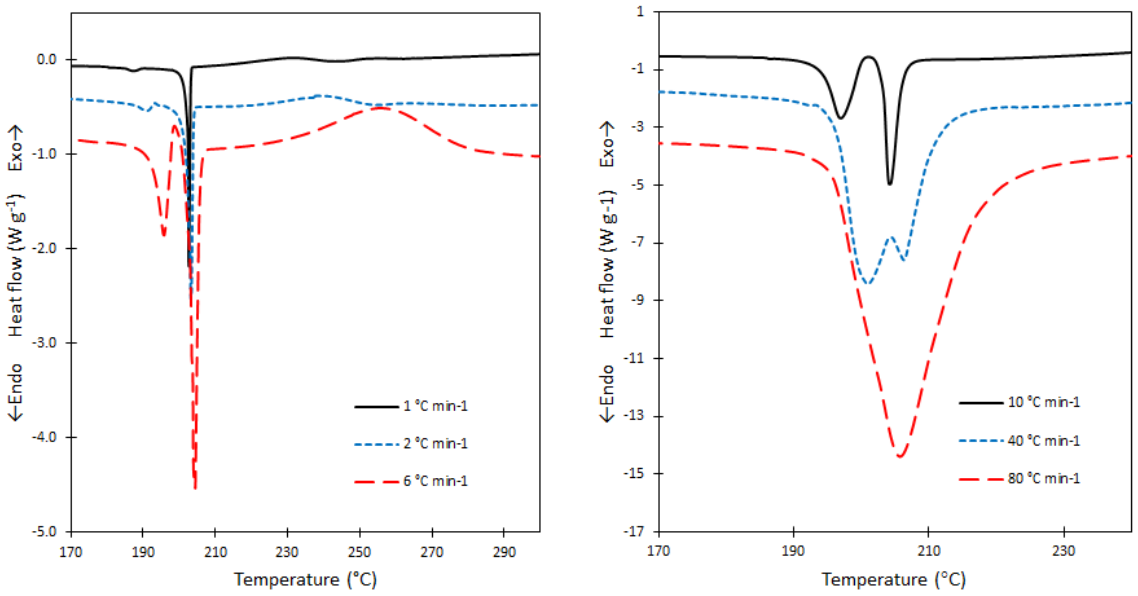

Figure 6.6. The effect of heating rate on the DSC curves for neat fipronil.

At low heating rates (1-2 °C min^{-1}), a small endotherm was observed at ~188 °C followed by a sharp melting peak centred at ~203 °C. As the heating rate was increased, the small endotherm at ~188 °C shifted to higher temperatures and increased in intensity. Simultaneously, the relative intensity of the second endotherm decreased. At intermediate heating rates (4-8 °C min^{-1}), two well-defined melting endotherms separated by a small exotherm were noticeable. At high heating rates (60-80 °C min^{-1}) the two melting endotherms merged until eventually only one broadened peak was left. This unexpected behaviour can be rationalised as follows. Polymorph CM-I (the lower melting form) is the metastable form which undergoes either a solid-solid transition or melting and recrystallization to the thermodynamically stable form, polymorph CM-V (the higher melting form). The metastable form has a finite existence due its slow rate of transformation into the stable form (Hilfiker, 2006). One explanation for the small

endotherm that was detected around 190 °C at lower heating rates (1-2 °C min^{-1}) is the occurrence of a solid phase transition CM-I → CM-V at a temperature well below the melting point of polymorph CM-I. When heated slowly, a low melting metastable polymorph usually transitions to the higher melting polymorph at an appropriate temperature. However, under rapid heating conditions it tends to overshoot and melt at its own melting point (Threlfall, 1995, Stephenson, 1973). Therefore, complete conversion of CM-I into the stable CM-V polymorph was only achieved at a low heating rate. At intermediate heating rates, the solid transformation CM-I → CM-V did not occur. Instead, CM-I melted. Once the metastable polymorph melted, the resulting melt crystallized to form the higher melting, stable polymorph CM-V. This explains the exotherm present at intermediate heating rates. This phenomenon can serve as another explanation for the small endotherm observed at around 190 °C at lower heating rates (1-2 °C min^{-1}). The gradual dissipation of the heat of fusion over time could have led to a recrystallization exotherm with a very low intensity that was undetectable on the DSC.

As the heating rate was increased further, less of the higher melting polymorph (CM-V) had time to form. This explains the variation in the relative intensities of the two melting endotherms with DSC heating rate (Fig. 6.6). It also explains why polymorph F-II reported by Zamir (2015) (cf. polymorph CM-I) appeared to have two melting points. It is simply an artefact caused by a solid-solid phase transformation of CM- I into CM-V, the stable polymorph. At a high heating rate of 80 °C min^{-1}, formation of the stable form was suppressed and only the melting endotherm of the metastable form was observed.

6.3.2 DSC analysis of the solvates

Representative DSC curves for the fipronil solvates, before and after heat-treatment, are shown in Fig. 6.7. The measured onset and peak temperatures are listed in Table 6.2. The results of the neat fipronil and the sublimation experiments were included for comparative purposes.

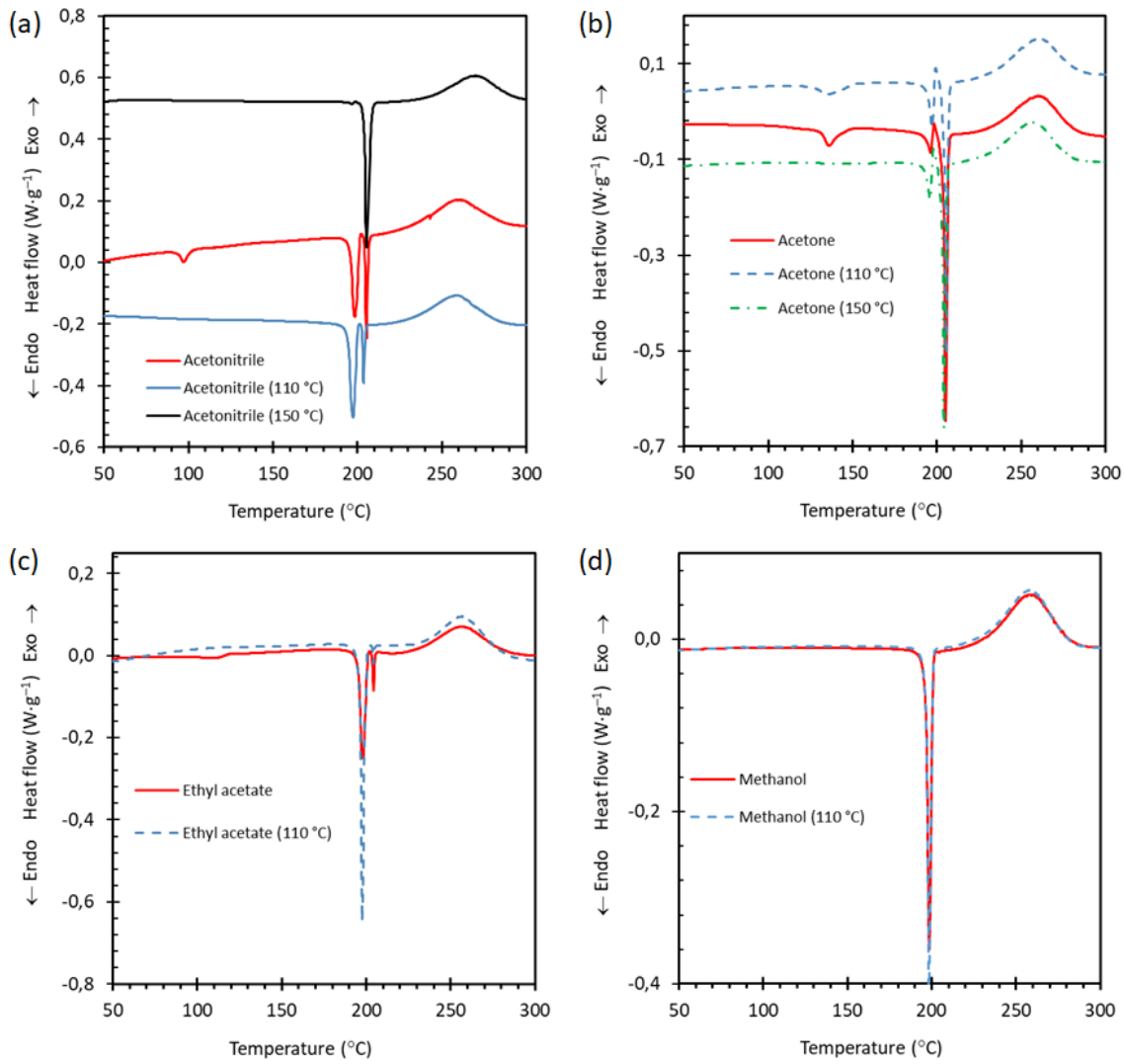

Figure 6.7. DSC curves obtained for fipronil samples prepared by recrystallization from (a) acetonitrile, (b) acetone, (c) ethyl acetate and (d) methanol, and after heating to either 110 °C and 150 °C. β = 5 °C min^{-1}.

Table 6.2. DSC parameters obtained for the neat and heat-treated fipronil, sublimate product and residue, as well as samples recrystallised from different solvents.

Sample	T_s onset (°C)	T_s peak (°C)	m.p. onset (°C)	T_{m1} (°C)	T_{m2} (°C)	ΔH_{m1} (J g^{-1})	ΔH_{m2} (J g^{-1})
Neat	-	-	193.2	197.0	205.8	21.2	87.1
Neat (150)*	-	-	193.8	196.3	204.6	17.3	89.9
Sublimate	-	-	193.3	195.4	-	96.8	-
Sublimate residue	-	-		-	206.1	-	95.3
Acetone	129.9	136.8	193.8	197.0	205.3	14.7	92.5
Acetone (110)	-	-	194.1	196.8	205.0	18.6	81.0
Acetonitrile	93.7	97.1	195.4	198.5	205.3	65.6	32.9
Acetonitrile (110)	-	-	193.6	197.4	203.6	90.7	19.5
Acetonitrile (150)	-	-	194.1	196.9	205.4	1.4	101.0
Ethyl acetate	-	-	196.4	198.1	-	78.2	-
Ethyl acetate (150)	-	-	194.7	-	206.0	-	101.5
Methanol	-	-	195.6	198.6	-	100.5	-
Methanol (110)	-	-	196.8	198.5	-	100.8	-

T_s: desolvation temperature; T_{m1} and ΔH_{m1}: peak temperature and enthalpy change associated with the first melting endotherm; T_{m2} and ΔH_{m2}: temperature and enthalpy change associated with the second melting endotherm. *: values in brackets indicate temperature of heat treatment in °C

Weak endothermic events were present in the DSC curves of some samples at temperatures below 150 °C. These endotherms reflected the release of the solvents, acetone, acetonitrile and ethyl acetate, present in the initial structures. The methanol-derived sample did not feature such an event.

At relatively high temperatures, all the samples exhibited a broad exotherm which peaked between 260 °C and 280 °C. This was attributed to the degradation of fipronil, also observed in the TGA experiments. The TGA results indicated that degradation of fipronil led to the loss

of volatile decomposition products and the formation of a thermally stable char residue (Fig. 6.3).

Fig. 6.7d shows that the methanol-derived sample is characterized by a single sharp melting endotherm with onset at 195.6 °C and peak temperature of 198.6 °C. The Figure shows that heat treatment of the methanol derived-sample at 110 °C for 10 min did not change the melting behaviour of this sample. In contrast, all the other examples, featured two melting endotherms with the second endotherm located at a temperature slightly higher than 200 °C. Both melting events featured quite sharp peaks but they varied in relative intensity for the different samples. For the acetone- and acetonitrile-derived samples (Fig 6.7a and b), the second melting event was most intense whereas the reverse held for ethyl acetate-derived sample (Fig 6.7c).

The effect of heat treatment of the acetonitrile-derived sample was particularly striking when comparing the DSC results of the sample before and after heat treatment. First compare the DSC curve for the solvate (Fig. 6.7a, red curve) and the sample heat treated at 110 °C (Fig. 6.7a, blue curve). The first endotherm became more intense following the heat treatment (ΔH_{m1} values 65.6 J g^{-1} *vs* 90.7 J g^{-1}; Table 6.2). However, when the acetonitrile-derived sample was heated for 30 min at 150 °C, the second melting event became dominant and only a vestige of the first remained (Fig. 6.7a, black curve). This was consistent with near complete transformation into the thermodynamically stable CM-V polymorph and implied that the solid-solid phase transformation temperature of the metastable polymorph must be below 150 °C.

The implication of the results presented above is that the ultimate phase morphology of fipronil depends on the solvents used in its preparation as well as on the thermal history it was subjected to. In order to investigate the latter, a series of heat-cool-reheat DSC runs were conducted. Fig. 6.8 shows typical behaviour observed for the different samples.

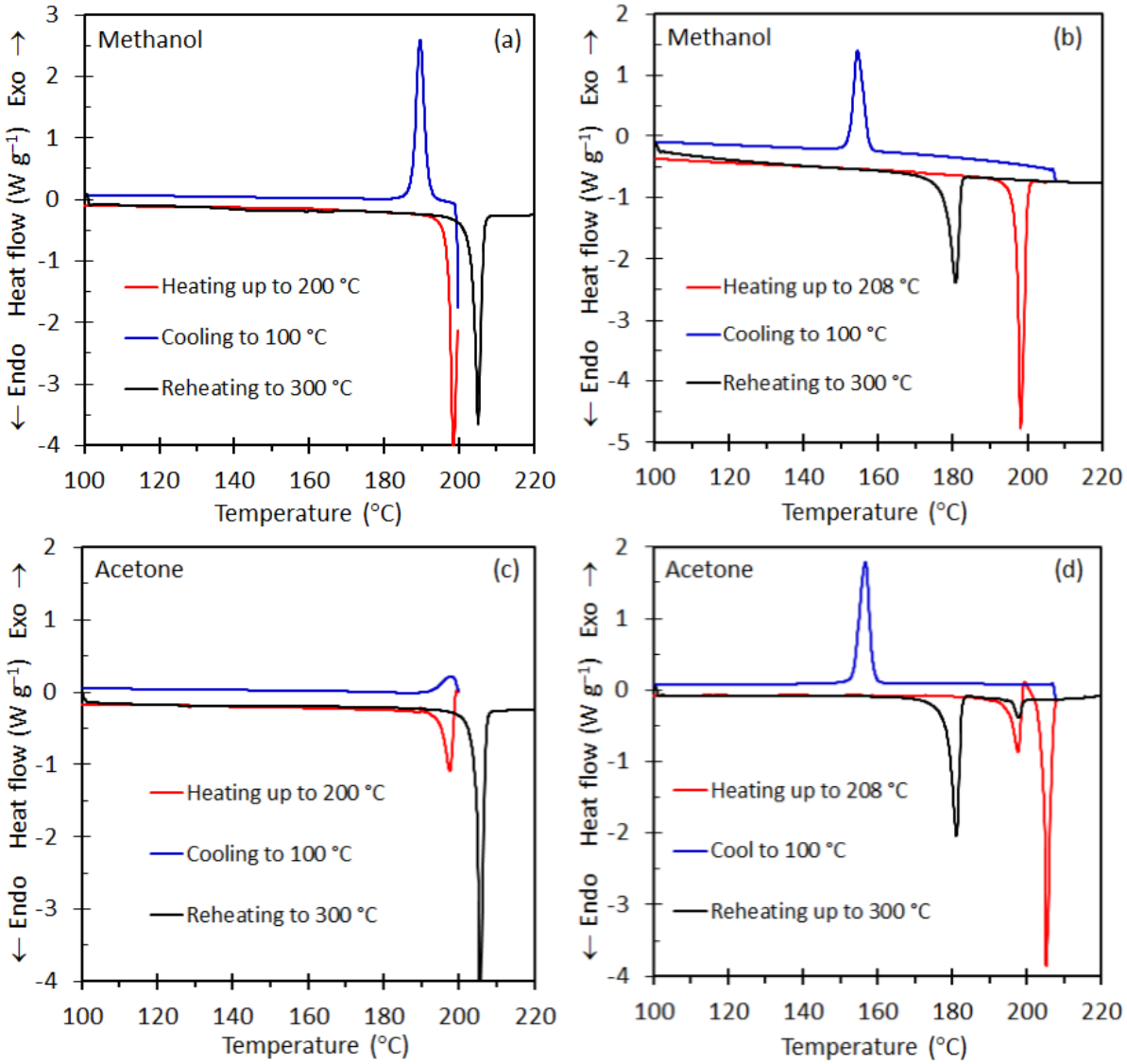

Figure 6.8. The effect of two different heat-cool-heat protocols on the DSC curves of fipronil samples obtained by recrystallization from methanol (a and b), and acetone (c and d). β = 5 °C min^{-1}.

In the first set of experiments, the samples were heated up to 200 °C, a temperature just beyond the first melting endotherm but before the onset of the second one, followed by immediate cooling down to 100 °C and then reheating to 300 °C. Heating any of the fipronil samples in this way resulted in them having only a single melting endotherm in the range 205 °C to 207 °C (Fig. 6.8a, c). This suggested that such a thermal treatment leads to an irreversible phase

transition of crystalline modification CM-I to crystalline modification CM-V, and confirmed that polymorph CM-V is the stable polymorph at elevated temperatures.

A similar procedure was carried out with the initial heating scan reaching 208 °C, a temperature just after the second endotherm (Fig. 6.8b, d). After rapidly cooling and then reheating, the DSC curve showed two endotherms, a major endotherm centred at 181.2 °C and a minor one centred at 197.3 °C. The minor endotherm at 197.3 °C corresponds to the melting range of polymorph CM-I while the endotherm at 181.2 °C is most likely due to a lower-melting degradation product of fipronil.

6.4 Conclusion

The DSC results, taken together with the TGA, PXRD and SCXRD results, indicated that neat fipronil was a mixture of two polymorphs, PM-5 and PM-1. PM-5 (cf. CM-I or F-II) is a metastable form which converts *via* a solid-solid phase transition into the higher melting, thermodynamically stable polymorph PM-1 (cf. CM-II or F-I) at temperatures well below its melting point of *ca.* 195 °C. The latter (PM-1) melts at *ca*. 206 °C and the enthalpy of melting is about 100 J g^{-1}. These observations explain the appearance of two melting endotherms in the DSC and the disappearance of the endotherm at lower temperatures when the heating rate is very slow, e.g. 1 °C min^{-1}. It also explains why heat treatment at 150 °C, of the sample prepared by recrystallization from acetonitrile, produced a near-pure polymorph PM-5.

Thermogravimetric analysis revealed that all recrystallized samples, except for the acetone-derived sample, were solvates. All of these pseudo-polymorphs exhibited solvent loss between 60 °C and 100 °C. The acetone-derived sample was found to be a hemihydrate exhibiting mass loss at 120 °C. Recrystallization from methanol did not yield a solvate, instead, a near-pure polymorph (PM-5) was formed.

Chapter 7

Conclusions

7.1 Overview

The aim of this study was to investigate the vaporization and polymorphic behaviour of fipronil by means of differential scanning calorimetry (DSC), thermogravimetric analysis (TGA), powder X-ray diffraction (PXRD) and single crystal X-ray diffraction (SCXRD). Isothermal TGA was employed to determine the sublimation and evaporation rates. From these measurements, vapour pressures were deduced on the assumption that the released vapours behaved like ideal gases and that mass loss was controlled by diffusion through the gas present in the partially filled crucible. For the latter process, the diffusion coefficient was estimated using the Fuller correlation. Results obtained using benzoic acid, as the calibration standard, suggested that it should be possible to estimate vapour pressures to within 12% with this TGA method. Several crystal forms were obtained from the neat, as-received fipronil by sublimation under vacuum and by recrystallization from different solvents. DSC results obtained at different scan rates and SCXRD analysis proved particularly useful in differentiating the different crystal forms of fipronil obtained. The results of the investigation vaporization and polymorphic behavior of fipronil are summarized below.

7.2 Conclusions

Objective 1: To determine the thermal characteristics of fipronil, specifically its sublimation and evaporation patterns at temperatures encountered during the conversion processes utilized to produce tri-layer films containing fipronil as the contact insecticide (Chapter 4 and 6).

DSC analysis of neat fipronil showed that neat fipronil had two melting endotherms at *ca*. 197 °C and 202 °C. Fipronil showed a tendency to sublime, evidenced by mass loss between 150 to 190 °C i.e. before the insecticide melted. Heating the sample beyond the melting temperature caused the fipronil to vaporize between 202-240 °C, and to decompose above 240 °C. A char residue remained and the amount depended on the heating rate used. Very little char residue remained at slow heating rates (1-2 °C/min), however, as the heating rate was increased the amount of char residue that remained also increased.

Objective 2: To extract the vapour pressure data and determine the enthalpies of sublimation and vaporization for fipronil from isothermal TGA curves.

The sublimation and evaporation processes followed zero-order kinetics. Sublimation of fipronil took place in the range 150–190 °C and the evaporation process in the range 195–220 °C. The vapour pressure data was estimated using the Clausius-Clapeyron vapour pressure equation. The standard enthalpies of sublimation and vaporization of fipronil were derived to be 120 ± 4 kJ mol^{-1} and 72 ± 5 kJ mol^{-1}, respectively, which in turn led to the value of 47.5 kJ mol^{-1} for the standard enthalpy of fusion. The data indicated that fipronil will likely sublime at polymer processing temperatures above 150 °C.

Objective 3: To isolate and characterise different crystal forms of fipronil through recrystallization from different solvents.

SCXRD analysis revealed the existence of five distinct forms of fipronil named polymorphs 1-5 (PM1-PM-5). PXRD analysis of the bulk samples obtained from different solvents confirmed the presence of several polymorphs. When crystallized from acetonitrile or ethyl acetate at room temperature, concomitant polymorphism was observed. Forms PM-1, PM-2, and PM-5 were obtained from the former solvent, while forms PM-1, PM-4, and PM-5 were obtained from the latter. Crystallization from acetone at room temperature exclusively yielded PM-3, while PM-5 was exclusively obtained from crystallization from methanol at room temperature. Pure PM-4 was obtained by cooling acetonitrile in a refrigerator and then crystallizing from it.

Recrystallization of fipronil from acetonitrile resulted in a mixture of different polymorphs or pseudo-polymorphs. However, subjecting the product to heat treatment for 30 minutes at 150 °C yielded a nearly pure polymorph that exhibited PXRD and thermal properties consistent with crystal modification CM-V described by Saxell et al. (2018) and form F-I reported by Zamir (2015). On the other hand, recrystallization from methanol did not produce a solvate, but instead yielded a near-pure polymorph referred to as PM-5. Its PXRD pattern was similar to that of crystal modification CM-I reported by Saxell et al. (2018) and Form F-II disclosed by Zamir (2015), and closely resembled the pattern predicted based on the single crystal data published by ark et al. (2017). All investigators agreed that this polymorph belongs to the monoclinic crystal system, but there were differences in space group indexing. While the present analysis indexes this polymorph into space group I2/a, Tang et al. (2005) suggested P21/n while both Saxell et al. (2013) and Park et al. (2017) indicated space group C2/c instead.

The crystal structures determined for the solvates PM-2, PM-3 and PM-4 showed a degree of similarity in terms of the packing of the molecules. However, the structures PM-1 and PM-5

were significantly different from each other, and from the rest of the structures. Of interest is the fact that, despite the structural differences, the same basic hydrogen bonding motif is present in all the structures.

Objective 4: To investigate the polymorphic behaviour of fipronil using a systematic comparison of thermochemical and structural properties of various crystal forms of fipronil obtained in this study and reported in the literature.

DSC analysis revealed the presence of two different crystal forms in the as-received neat fipronil. Pure samples of these two forms were obtained via vacuum sublimation. The metastable, lower melting polymorph, and the thermodynamically stable, higher melting polymorph melted at approximately 196 °C and 205 °C, respectively. Careful analysis of the DSC results, obtained at different temperature scan rates, showed that the lower melting polymorph converted to the higher melting form via a solid-solid phase transition.

The crystallography and thermal properties of fipronil polymorphs and pseudo-polymorphs in the hope of finding a resolution to the differences in what is reported in literature. Five different crystal forms of fipronil were identified by SCXRD analysis. Concomitant polymorphism was observed when fipronil was crystallized from acetonitrile or ethyl acetate at room temperature. Forms PM-1, PM-2 and PM-5 crystallized from the first solvent, and forms PM-1, PM-4 and PM-5 from the second. Crystallization from acetone at room temperature was found to exclusively yield PM-3, while PM-5 was exclusively obtained from crystallization from methanol at room temperature. Pure PM-4 was obtained by crystallizing from acetonitrile cooled in a refrigerator. Thermogravimetric analysis revealed that all five forms, except for the acetone-derived sample, were solvates. All of these pseudo-polymorphs exhibited solvent loss between 60 °C and 100 °C. The acetone-derived sample was found to be a hemihydrate

exhibiting mass loss at 120 °C. Recrystallization from methanol did not yield a solvate, instead, a near-pure polymorph (PM-5) was formed.

Despite recrystallization from acetonitrile giving a mixture of different polymorphs/pseudo-polymorphs, heat treating this product for 30 min at 150 °C resulted in a near-pure polymorph with PXRD and thermal behaviour consistent with crystal modification CM-V described by Saxell et al. (2018) and form F-I reported by Zamir (2015). The methanol-derived form, PM-5, had similar PXRD properties to those for crystal modification CM-I reported by Saxell et al. (2013) and Form F-II disclosed by Zamir (2015). Its PXRD pattern also closely resembled the one predicted on the basis of the single crystal data published by Park et al. (2017). All investigators agreed that this polymorph belongs in the monoclinic crystal system. However, the present analysis indexes this polymorph into space group *I*2/*a* whereas Tang et al. (2005) suggested $P2_1/n$ and both Saxell et al. (2013) and Park et al. (2017) indicated space group *C*2/*c* instead.

The DSC results, taken together with the TGA, PXRD and SCXRD results, indicated that PM-5 (cf. CM-I or F-II) is the metastable form and converts via a solid-solid phase transition into the higher melting, thermodynamically stable polymorph PM-1 (cf. CM-V or F-I) at temperatures well below its melting point of *ca.* 195 °C. The latter (PM-1) melts at *ca.* 206 °C and the enthalpy of melting is about 100 J g^{-1}. These observations explain the appearance of two melting endotherms in the DSC and the disappearance of the endotherm at lower temperatures when the heating rate is very slow, e.g. 1 °C min^{-1}. It also explains why heat treatment at 150 °C, of the sample prepared by recrystallization from acetonitrile, produced a near-pure polymorph CM-1.

7.3 Recommendations for future work

The following recommendations are made for future studies in order to better understand the thermal and structural properties of fipronil.

- optimize the crystallization conditions when obtaining the various crystal form of fipronil.
- separate and purify of the mixtures of fipronil crystal forms obtained from recrystallization.
- investigate concomitant thermophysical transitions, such as pre-melting and onset of thermochemical degradation in the mass loss data.
- investigate the effect of varying the heating rate used to reach the isothermal temperature during TGA measurements.
- investigate the gaseous products of fipronil degradation by TG_FTIR or TG-MS and the residues by HPLC-MS.

References

AÏKPON, R., SÈZONLIN, M., TOKPONON, F., OKÈ, M., OUSSOU, O., OKÉ-AGBO, F., BEACH, R. & AKOGBÉTO, M. 2014. Good performances but short lasting efficacy of Actellic 50 EC Indoor Residual Spraying (IRS) on malaria transmission in Benin, West Africa. *Parasites & vectors,* 7**,** 1-8.

ARIEY, F., GAY, F. & MÉNARD, R. 2019. *Malaria Control and Elimination,* Springer.

ARONHIME, J. S. 1988. Application of thermal analysis (DSC) in the study of polymorphic transformations. *Thermochimica Acta,* 134**,** 1-14.

BARNES, K. I. 2011. Antimalarial drugs and the control and elimination of malaria. *Treatment and prevention of malaria.* Springer.

BECKER, N., PETRIĆ, D., ZGOMBA, M., BOASE, C., MADON, M., DAHL, C. & KAISER, A. 2010. Mosquitoes and their control. *Springer Science & Business Media,* 577.

BERNSTEIN, J., DAVEY, R. J. & HENCK, J. O. 1999. Concomitant polymorphs. *Angewandte Chemie International Edition,* 38**,** 3440-3461.

BEVERLEY, K. J., CLINT, J. H. & FLETCHER, P. D. I. 1999. Evaporation rates of pure liquids measured using a gravimetric technique. *Physical Chemistry Chemical Physics,* 1**,** 149-153.

BHATIA, A., CHOPRA, S., NAGPAL, K., DEB, P. K., TEKADE, M. & TEKADE, R. K. 2018. Chapter 2 - Polymorphism and its Implications in Pharmaceutical Product Development. *In:* TEKADE, R. K. (ed.) *Dosage Form Design Parameters.* Academic Press.

BREMAN, J. G., KILAMA, W. L., GREENWOOD, B., DRUILHE, P., NABARRO, D. & MENDIS, K. 2000. Rolling back malaria: action or rhetoric? : SciELO Public Health.

BROWN, M. E. 2001. *Introduction to thermal analysis: techniques and applications,* Springer.

CARTER, R. & MENDIS, K. N. 2002. Evolutionary and historical aspects of the burden of malaria. *Clinical microbiology reviews,* 15**,** 564-594.

COWMAN, A. F., BERRY, D. & BAUM, J. 2012. The cellular and molecular basis for malaria parasite invasion of the human red blood cell. *Journal of cell Biology,* 198**,** 961-971.

CURTIS, C. 1996. Impregnated bednets, malaria control and child mortality in Africa. *Tropical medicine & international health: TM & IH,* 1**,** 137.

DAVEY, R. J. 2002. Polymorphism in Molecular Crystals Joel Bernstein. Oxford University Press, New York, 2002. ISBN 0198506058. ACS Publications.

DELLE SITE, A. 1997. The vapor pressure of environmentally significant organic chemicals: a review of methods and data at ambient temperature. *Journal of Physical and Chemical Reference Data,* 26**,** 157-193.

DUNITZ, J. D. & BERNSTEIN, J. 1995. Disappearing polymorphs. *Accounts of chemical research,* 28**,** 193-200.

ELDER, J. 1997. Sublimation measurements of pharmaceutical compounds by isothermal thermogravivletry. *Journal of Thermal Analysis and Calorimetry,* 49**,** 897-905.

FARRUGIA, L. J. 2012. WinGX and ORTEP for Windows: an update. *Journal of Applied Crystallography,* 45**,** 849-854.

GARI, T. & LINDTJØRN, B. 2018. Reshaping the vector control strategy for malaria elimination in Ethiopia in the context of current evidence and new tools: opportunities and challenges. *Malaria journal,* 17**,** 1-8.

GAUR, D., CHITNIS, C. E. & CHAUHAN, V. S. 2016. *Advances in malaria research,* John Wiley & Sons.

GIRON, D. 1995. Thermal analysis and calorimetric methods in the characterisation of polymorphs and solvates. *Thermochimica acta,* 248**,** 1-59.

GOEL, A., MCCONNELL, L. L. & TORRENTS, A. 2007. Determination of vapor pressure-temperature relationships of current–use pesticides and transformation products. *Journal of Environmental Science and Health Part B,* 42**,** 343-349.

GOLDSMITH, C. 2010. *Battling Malaria: On the Front Lines Against a Global Killer*, Twenty-First Century Books.

GOLS, R., WALLISDEVRIES, M. F. & VAN LOON, J. J. 2020. Reprotoxic effects of the systemic insecticide fipronil on the butterfly Pieris brassicae. *Proceedings of the Royal Society B,* 287**,** 20192665.

GRUNENBERG, A. 1997. Polymorphie und thermische Analyse pharmazeutischer Wirkstoffe. *Pharmazie in unserer Zeit,* 26**,** 224-231.

GRUNENBERG, A., HENCK, J.-O. & SIESLER, H. W. 1996. Theoretical derivation and practical application of energy/temperature diagrams as an instrument in preformulation studies of polymorphic drug substances. *International Journal of Pharmaceutics,* 129**,** 147-158.

GÜCKEL, W., KÄSTEL, R., KRÖHL, T. & PARG, A. 1995. Methods for determining the vapour pressure of active ingredients used in crop protection. Part IV. An improved thermogravimetric determination based on evaporation rate. *Pesticide science,* 45**,** 27-31.

GUPTA, R. C. & ANADÓN, A. 2018. Fipronil. *Veterinary Toxicology.* Elsevier.

HILFIKER, R. 2006. *Polymorphism: in the Pharmaceutical Industry.*, Weinheim, Wiley-VCH Verlag GmbH & Co. KGaA.

HILL, J., LINES, J. & ROWLAND, M. 2006. Insecticide-treated nets. *Advances in parasitology,* 61**,** 77-128.

JACKSON, D., CORNELL, C., LUUKINEN, B., BUHL, K. & STONE, D. 2009. Fipronil technical fact sheet. *National Pesticide Information Center, Oregon State University Extension Services*.

JENNINGS, S. G. 1988. The mean free path in air. *Journal of Aerosol Science,* 19**,** 159-166.

KARUNAMOORTHI, K. 2011. Vector control: a cornerstone in the malaria elimination campaign. *Clinical Microbiology and Infection,* 17**,** 1608-1616.

KILLEEN, G. F. 2020. Control of malaria vectors and management of insecticide resistance through universal coverage with next-generation insecticide-treated nets. *Lancet (London, England)*.

KILLEEN, G. F., SMITH, T. A., FERGUSON, H. M., MSHINDA, H., ABDULLA, S., LENGELER, C. & KACHUR, S. P. 2007. Preventing childhood malaria in Africa by protecting adults from mosquitoes with insecticide-treated nets. *PLoS medicine,* 4.

KLIMENKO, A. 2012. Teaching the third law of thermodynamics. *arXiv preprint arXiv:1208.4189*.

KUMAR, N., KUMAR, R., SHAKIL, N. A., SARKAR, D. J. & CHANDER, S. 2019. Evaluation of fipronil nanoformulations for effective management of brown plant hopper (Nilaparvata lugens) in rice. *International Journal of Pest Management,* 65**,** 86-93.

LANGMUIR, I. 1913. The vapor pressure of metallic tungsten. *Physical Review,* 2**,** 329-342.

LEE, E. H. 2014. A practical guide to pharmaceutical polymorph screening & selection. *Asian Journal of Pharmaceutical Sciences,* 9**,** 163-175.

LENGELER, C., CATTANI, J. & DE SAVIGNY, D. 1996. *Net Gain: a new method for preventing malaria deaths*, Idrc.

LENGELER, C., GRABOWSKY, M., MCGUIRE, D. & DESAVIGNY, D. 2007. Quick wins versus sustainability: options for the upscaling of insecticide-treated nets. *Defining and*

Defeating the Intolerable Burden of Malaria III: Progress and Perspectives: Supplement to Volume 77 (6) of American Journal of Tropical Medicine and Hygiene.

LOHANI, S. & GRANT, D. J. 2006. Thermodynamics of polymorphs. *Polymorphism: In the pharmaceutical industry***,** 21-42.

MACRAE, C. F., EDGINGTON, P. R., MCCABE, P., PIDCOCK, E., SHIELDS, G. P., TAYLOR, R., TOWLER, M. & STREEK, J. 2006. Mercury: visualization and analysis of crystal structures. *Journal of applied crystallography,* 39**,** 453-457.

MADZORERA, T., SIBANDA, M., FOCKE, W., MADITO, M. & MANYALA, N. 2019. Malathion-filled trilayer polyolefin film for malaria vector control. *Materials Science and Engineering: C,* 96**,** 419-425.

MAPOSSA, A. B., MOYO, D., WESLEY-SMITH, J., FOCKE, W. W. & ANDROSCH, R. Blooming of chlorfenapyr from polyethylene films. AIP Conference Proceedings, 2020. AIP Publishing LLC, 020036.

MAPOSSA, A. B., SIBANDA, M. M., MOYO, D., KRUGER, T., FOCKE, W. W., ANDROSCH, R., BOLDT, R. & WESLEY-SMITH, J. 2021. Blooming of insecticides from polyethylene mesh and film. *Transactions of the Royal Society of South Africa,* 76**,** 127-136.

MARGARIDO, T. C. S., FELÍCIO, A. A., DE CERQUEIRA ROSSA-FERES, D. & DE ALMEIDA, E. A. 2013. Biochemical biomarkers in Scinax fuscovarius tadpoles exposed to a commercial formulation of the pesticide fipronil. *Marine environmental research,* 91**,** 61-67.

MENDIS, K., RIETVELD, A., WARSAME, M., BOSMAN, A., GREENWOOD, B. & WERNSDORFER, W. H. 2009. From malaria control to eradication: The WHO perspective. *Tropical Medicine & International Health,* 14**,** 802-809.

MENON, D., DOLLIMORE, D. & ALEXANDER, K. S. 2002. A TG–DTA study of the sublimation of nicotinic acid. *Thermochimica acta*, 392**,** 237-241.

MILLER, L. H., GOOD, M. F. & MILON, G. 1994. Malaria pathogenesis. *Science*, 264**,** 1878-1883.

MILNER, D. A. 2018. Malaria pathogenesis. *Cold Spring Harbor perspectives in medicine*, 8**,** a025569.

MONTE, M. J., SANTOS, L. M., FULEM, M., FONSECA, J. M. & SOUSA, C. A. 2006. New static apparatus and vapor pressure of reference materials: naphthalene, benzoic acid, benzophenone, and ferrocene. *Journal of Chemical & Engineering Data*, 51**,** 757-766.

MORAES, B., MENEZES, C., LEITEMPERGER, J., DO AMARAL, A. M. B., LORO, V. L. & CLASEN, B. 2020. Comparative Study on Diet Added with Organic and Inorganic Selenium Forms Provided to Carps Exposed to Fipronil Insecticide. *Water, Air, & Soil Pollution*, 231**,** 1-12.

NAJERA, J. & ZAIM, M. 2001. *Malaria vector control*, World Health Organization, WHO.

NÁJERA, J. A., GONZÁLEZ-SILVA, M. & ALONSO, P. L. 2011. Some lessons for the future from the Global Malaria Eradication Programme (1955–1969). *PLoS medicine*, 8.

OLENIK, B. & THIELKING, G. 2012. Polymorphism and the organic solid state: influence on the optimization of agrochemicals. *Modern Methods in Crop Protection Research*, 10**,** 249-272.

PARK, H., KIM, J., KWON, E. & KIM, T. H. 2017. Crystal structure of fipronil. *Acta Crystallographica Section E: Crystallographic Communications*, 73**,** 1472-1474.

PARKER, A. & BABAS, R. 2014. Thermogravimetric measurement of evaporation: Data analysis based on the Stefan tube. *Thermochimica Acta*, 595**,** 67-73.

PERRENOT, B. & WIDMANN, G. 1994. Polymorphism by differential scanning calorimetry. *Thermochimica acta*, 234**,** 31-39.

PHANG, P. & DOLLIMORE, D. 2001. The calculation of the vapor pressures of antioxidants over a range of temperatures using thermogravimetry. *Thermochimica Acta,* 367-368**,** 263-271.

PIETERSE, N. & FOCKE, W. W. 2003. Diffusion-controlled evaporation through a stagnant gas: Estimating low vapour pressures from thermogravimetric data. *Thermochimica Acta,* 406**,** 191-198.

PLUESS, B., TANSER, F. C., LENGELER, C. & SHARP, B. L. 2010. Indoor residual spraying for preventing malaria. *Cochrane database of systematic reviews*.

POLING, B. E., PRAUSNITZ, J. M. & O'CONNELL, J. P. 2001. *Properties of gases and liquids*, McGraw-Hill Education.

PREMKUMAR, P. A., PANKAJAVALLI, R., SREEDHARAN, O., RAGHUNATHAN, V., NAGARAJA, K. & MALLIKA, C. 2004. Determination of vapour pressure and standard enthalpies of sublimation and vapourisation of N, N′-ethylenebis (2, 4-pentanedion-iminoato) nickel (II) by a TG-based transpiration method. *Materials Letters,* 58**,** 2256-2260.

PRICE, D. M. 2001. Vapor pressure determination by thermogravimetry. *Thermochimica acta,* 367**,** 253-262.

RAGHAVENDRA, K., BARIK, T. K., REDDY, B., SHARMA, P. & DASH, A. P. 2011. Malaria vector control: from past to future. *Parasitology research,* 108**,** 757-779.

RIGAKU, O. 2018. *CrysAlis PRO Software system,* Oxford, UK, Rigaku Corporation.

RONG, Y., GREGSON, C. M. & PARKER, A. 2012. Thermogravimetric measurements of liquid vapor pressure. *Journal of Chemical Thermodynamics,* 51**,** 25-30.

ROY, S., AITIPAMULA, S. & NANGIA, A. 2005. Thermochemical analysis of venlafaxine hydrochloride polymorphs 1− 5. *Crystal growth & design,* 5**,** 2268-2276.

RUZ, V., GONZÁLEZ, M. M., WINANT, D., RODRÍGUEZ, Z. & VAN DEN MOOTER, G. 2015. Characterization of the sublimation and vapor pressure of 2-(2-nitrovinyl) furan (G-0) using thermogravimetric analysis: effects of complexation with cyclodextrins. *Molecules,* 20**,** 15175-15191.

SAXELL, H. E., ERK, P., TARANTA, C., KRÖHL, T., COX, G., DESIRAJU, G. R., BANERJEE, R. & BHATT, P. M. 2011. *Crystalline modification of fipronil, US 8,063,092 B2*.

SAXELL, H. E., ERK, P., TARANTA, C., KRÖHL, T., COX, G., DESIRAJU, G. R., BANERJEE, R. & BHATT, P. M. 2014. *Crystalline modification of fipronil, US 8,791,046 B2*.

SAXELL, H. E., ERK, P., TARANTA, C., KRÖHL, T., COX, G., SUKOPP, M., DESIRAJU, G. R., BANERJEE, R. & BHATT, P. M. 2012. Crystalline modification of fipronil. Google Patents.

SAXELL, H. E., ERK, P., TARANTA, C., KRÖHL, T., COX, G., SUKOPP, M., DESIRAJU, G. R., BANERJEE, R. & BHATT, P. M. 2018. *Crystalline modification of fipronil, US 8,913,473 B2*.

SAXELL, H. E., ERK, P., TARANTA, C., KRÖHL, T., COX, G., SUKOPP, M., SCHERER, S., OJALA, A., DESIRAJU, G. R., BANERJEE, R. & BHATT, P. M. 2013. *Crystalline modification of fipronil, US 8,383,664 B2*.

SHELDRICK, G. M. 2015. SHELXT–Integrated space-group and crystal-structure determination. *Acta Crystallographica Section A: Foundations and Advances,* 71**,** 3-8.

SHIFF, C. 2002. Integrated approach to malaria control. *Clinical microbiology reviews,* 15**,** 278-293.

SIMON-DELSO, N., AMARAL-ROGERS, V., BELZUNCES, L. P., BONMATIN, J. M., CHAGNON, M., DOWNS, C., FURLAN, L., GIBBONS, D. W., GIORIO, C.,

GIROLAMI, V., GOULSON, D., KREUTZWEISER, D. P., KRUPKE, C. H., LIESS, M., LONG, E., MCFIELD, M., MINEAU, P., MITCHELL, E. A. D., MORRISSEY, C. A., NOOME, D. A., PISA, L., SETTELE, J., STARK, J. D., TAPPARO, A., VAN DYCK, H., VAN PRAAGH, J., VAN DER SLUIJS, J. P., WHITEHORN, P. R. & WIEMERS, M. 2015. Systemic insecticides (neonicotinoids and fipronil): trends, uses, mode of action and metabolites. *Environmental Science and Pollution Research,* 22**,** 5-34.

SINGH, N. S., SHARMA, R., PARWEEN, T. & PATANJALI, P. 2018. Pesticide contamination and human health risk factor. *Modern age environmental problems and their remediation.* Springer.

SINGH, N. S., SHARMA, R., PARWEEN, T. & PATANJALI, P. K. 2017. Pesticide contamination and human health risk factor. *Modern Age Environmental Problems and their Remediation.*

SONNEFELD, W., ZOLLER, W. & MAY, W. 1983. Dynamic coupled-column liquid-chromatographic determination of ambient-temperature vapor pressures of polynuclear aromatic hydrocarbons. *Analytical chemistry,* 55**,** 275-280.

STEPHENSON, W. 1973. M. Kuhnert-Brandstätter, Thermomicroscopy in the analysis of pharmaceuticals: International Series of Monographs in Analytical Chemistry, Vol. 45, Pergamon Press, Oxford, 1971, 409 pp.: Elsevier.

SZCZOTOK, A. M., KJØNIKSEN, A. L., RODRIGUEZ, J. F. & CARMONA, M. 2019. The accurate diffusive model for predicting the vapor pressure of phase change materials by thermogravimetric analysis. *Thermochimica Acta,* 676**,** 64-70.

TAKKEN, W. & KNOLS, B. G. 2009. Malaria vector control: current and future strategies. *Trends in parasitology,* 25**,** 101-104.

TANG, R.-Y., ZHONG, P., LIN, Q.-L., HU, M.-L. & SHI, Q. 2005. 5-Amino-1-[2,6-dichloro-4-(trifluoromethyl)phenyl]-4-(trifluoromethylsulfanyl)-1H-pyrazole-3-carbonitrile. *Acta Crystallographica Section E,* 61**,** o4374-o4375.

TANGPUKDEE, N., DUANGDEE, C., WILAIRATANA, P. & KRUDSOOD, S. 2009. Malaria diagnosis: a brief review. *The Korean journal of parasitology,* 47**,** 93.

TANNER, M. & SAVIGNY, D. D. 2008. Malaria eradication back on the table. SciELO Public Health.

THRELFALL, T. L. 1995. Analysis of organic polymorphs. A review. *Analyst,* 120**,** 2435-2460.

TINGLE, C. C., ROTHER, J. A., DEWHURST, C. F., LAUER, S. & KING, W. J. 2003. Fipronil: environmental fate, ecotoxicology, and human health concerns. *Reviews of environmental contamination and toxicology.* Springer.

TUTEJA, R. 2007. Malaria− an overview. *The FEBS journal,* 274**,** 4670-4679.

VAN GENDEREN, A. C. & OONK, H. A. 2003. The (solid+ vapor) equilibrium. A view from the arc. *Colloids and Surfaces A: Physicochemical and Engineering Aspects,* 213**,** 107-115.

WIEDEMANN, H. 1972. Applications of thermogravimetry for vapor pressure determination. *Thermochimica Acta,* 3**,** 355-366.

WISNIAK, J. 2001. Historical development of the vapor pressure equation from Dalton to Antoine. *Journal of phase equilibria,* 22**,** 622.

WORLD HEALTH ORGANIZATION. 1999. Roll back malaria: report by the director-general. *52nd World health assembly. 14 April 1999.*

WORLD HEALTH ORGANIZATION. 2015a. *Indoor residual spraying: an operational manual for indoor residual spraying (IRS) for malaria transmission control and elimination,* World Health Organization.

WORLD HEALTH ORGANIZATION. 2015b. World Malaria Report (2015), World Health Organization. *Geneva, Switzerland*.

WORLD HEALTH ORGANIZATION. 2016. *World malaria report 2015*, World Health Organization.

WORLD HEALTH ORGANIZATION. 2019. *Guidelines for malaria vector control*, World Health Organization.

WORLD HEALTH ORGANIZATION. 2021. *World malaria report 2021*, World Health Organization.

WRIGHT, S., PHANG, P., DOLLIMORE, D. & ALEXANDER, K. 2002. An overview of calibration materials used in thermal analysis—benzoic acid. *Thermochimica acta*, 392**,** 251-257.

ZAMIR, S. 2013. *Polymorphs and amorphous forms of 5-amino-1[2,6-dichloro-4-(trifluoromethyl)phenyl]-4-[(trifluoromethyl)sulfinyl]-1H-pyrazole-carbonitrile, US 8,440,709 B2*.

ZAMIR, S. 2015. *Polymorphs and amorphous forms of 5-amino-1[2,6-dichloro-4-(trifluoromethyl)phenyl]-4-[(trifluoromethyl)sulfinyl]-1H-pyrazole-carbonitrile, US 9,215,873 B2*.

ZGHAL, I., FARJAS, J., CAMPS, J., DAMMAK, M. & ROURA, P. 2018. Thermogravimetric measurement of the equilibrium vapour pressure: Application to water and triethanolamine. *Thermochimica Acta*, 665**,** 92-101.

Appendix

Alternative method for vapour pressure estimation using the Eyring equation.

The fitting of the regression data from the isothermal TGA curves to the Eyring equation is shown in Fig. A1. The slope of each isothermal TG curve was used to determine the sublimation/evaporation rate of fipronil at each temperature. The enthalpy of sublimation and the entropy of sublimation can be obtained from the slope and the intercept of the linear form of the Eyring equation. The activation enthalpy of fipronil sublimation was calculated from the slope of a linear regression line with correlation coefficient (r^2) of 0.9978. The sublimation enthalpy (from 150 °C to 190 °C) was 122.2 kJ mol^{-1} and the enthalpy of evaporation (from 195 °C to 220 °C) was 91.1 kJ mol^{-1}. Based on Hess's Law, the difference between the enthalpy of sublimation and evaporation is the heat of fusion, which is 31.1 kJ mol^{-1}. The entropy of sublimation and evaporation were found to be 267.7 kJ.mol^{-1} and 203.3 kJ mol^{-1}, respectively.

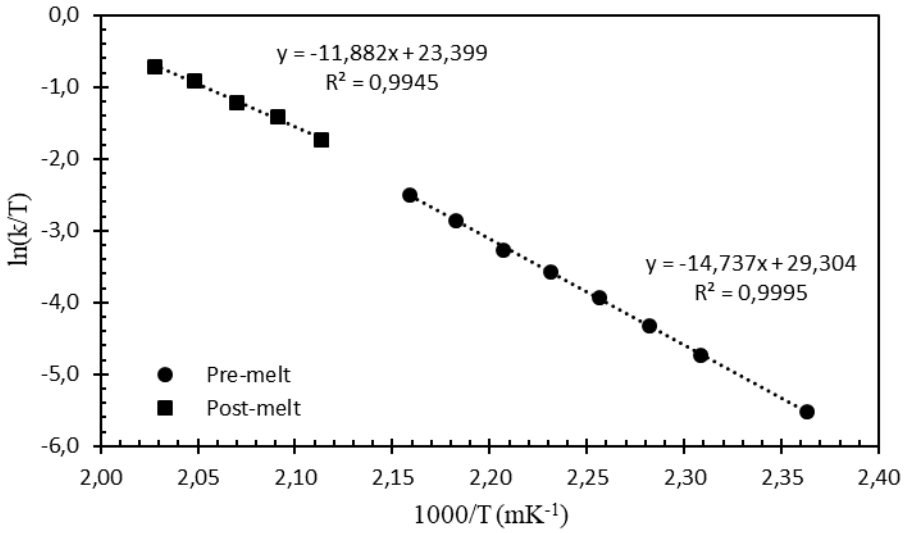

Figure A1. The Eyring plot for fipronil vaporization process below and above the melting point.

Vapour pressure estimation

The logarithm of sublimation/evaporation at a specific temperature is linearly proportional to the logarithm of pressure and obeys the equation;

$$Ln(P) = a * Ln(k) + b \quad (1)$$

where P is the vapour pressure at a given temperature, and k is the rate of sublimation or evaporation at this temperature. a and b are constants specific to a given instrument and set of experimental conditions and procedures but independent of the material used. The linear relationship between sublimation rate and vapour pressure is independent of the material used and the temperature range in which the experiments are carried out but is dependent on the specific instrumental system, experimental conditions, and sample containment procedure (Ruz et al., 2015).

Benzoic acid was used as a reference standard for vapour pressure estimation by TGA. The same method and instrumental configuration used for fipronil were used for the determination

of the isothermal sublimation rates (*dm/dt*) of benzoic acid over a temperature range of 40 °C to 70 °C at 5 °C increments. The data is shown in Table A1. This data obeys the Eyring rate equation (2) with 0.9996 correlation coefficient.

$$\ln\left(\frac{k}{T}\right) = -\frac{\Delta H}{RT} + \frac{\Delta S}{R} \qquad (2)$$

Table A1. Experimentally determined sublimation rate of benzoic acid between 40 °C and 70 °C on the TGA system used in this study and the published vapour pressure at each corresponding temperature.

Temperature (°C)	Sublimation rate, µg min^{-1}	Vapour pressure, Pa*
40	0.8	0.910
45	1.4	1.546
50	2.4	2.582
55	5.1	4.245
60	7.6	6.878
65	12.2	10.985
70	20.2	17.306

*Calculated using data of Wiedemann (Wiedemann, 1972)

The sublimation enthalpy, ΔH_s = 96.8 kJ mol^{-1}, is in reasonably good agreement with literature values computed from the Clausius–Clapeyron equation (Wiedemann, 1972). This means that, for purposes of estimation, the vapour pressure data can be extrapolated to the temperature range used in this study. The extrapolated vapour pressure values are also shown in Table A1. A plot of the sublimation rates of benzoic acid versus the published vapour pressure at each temperature is shown in Fig. A2.

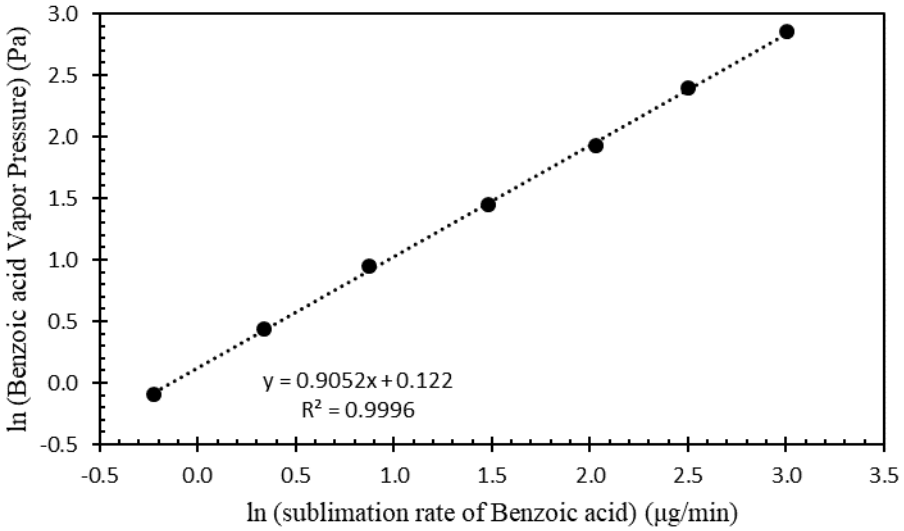

Figure A2. The linear logarithmic relationship between the sublimation rate of benzoic acid and the corresponding vapour pressure reported in literature.

Linearly regression of the vapour pressure and the sublimation rate data give;

$$\ln(p) = 0.9052 \cdot \ln(dm/dt) + 0.122 \quad (3)$$

Equation (4) was used to estimate vapour pressure values from the sublimation rates of fipronil in the temperature range 150–190 °C and these are listed in Table A2.

$$p' = \frac{WRT}{MV_c} \quad (4)$$

The pressure versus temperature plot for fipronil was obtained (Fig. A3). Fipronil exhibits an estimated vapour pressure of 3.32×10^{-8} kPa.

Table A2. Fipronil sublimation rates and estimated vapour pressures.

Temperature (°C)	*dm/dt* (µg min^{-1})	"Estimated" p (Pa)
150	32.2	26.18
160	74.7	56.07
165	121.2	86.89
170	177	122.42
175	240.9	161.82
180	348.9	226.28
185	523.6	326.76
190	710.8	430.91

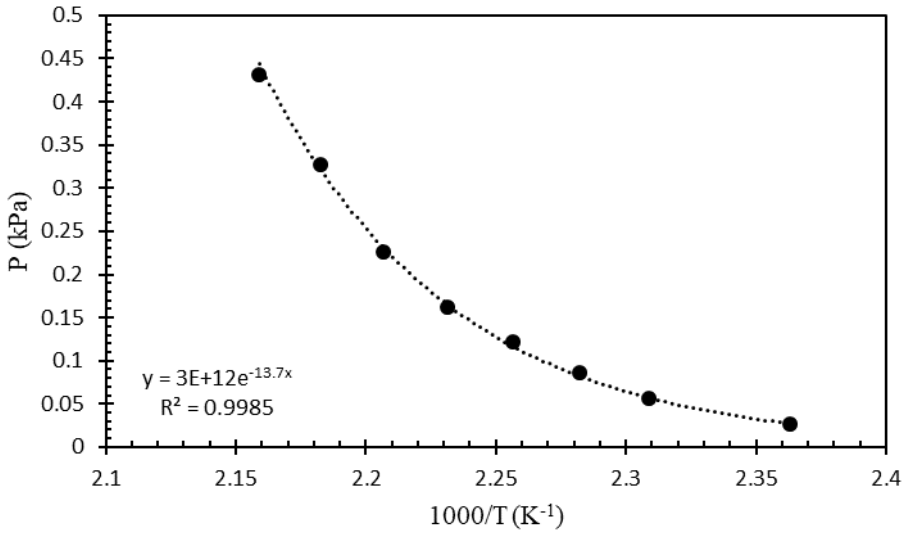

Figure A3. Vapour pressure plot for fipronil.